# REPORT DOCUMENTATION PAGE

Form Approved
OMB No. 074-0188



| 1. AGENCY USE ONLY (Leave blank) | 2. REPORT DATE | 3. REPORT TYPE AND DATE COVERED |
|---|---|---|
| | 4 May 2007 | |

**4. TITLE AND SUBTITLE**
Simulation and Evaluation of Marine Propeller Crashback Through Computational Fluid Dynamics

**5. FUNDING NUMBERS**

**6. AUTHOR(S)**
**Shearer, Matthew P.**

| 7. PERFORMING ORGANIZATION NAME(S) AND ADDRESS(ES) | | 8. PERFORMING ORGANIZATION REPORT NUMBER |
|---|---|---|
| | | |

| 9. SPONSORING/MONITORING AGENCY NAME(S) AND ADDRESS(ES) | | 10. SPONSORING/MONITORING AGENCY REPORT NUMBER |
|---|---|---|
| **US Naval Academy<br>Annapolis, MD 21402** | | **Trident Scholar project report no. 358 (2007)** |

**11. SUPPLEMENTARY NOTES**

| 12a. DISTRIBUTION/AVAILABILITY STATEMENT | 12b. DISTRIBUTION CODE |
|---|---|
| **This document has been approved for public release; its distribution is UNLIMITED.** | |

**13. ABSTRACT** Crashback is a maneuver which occurs when a ship or submarine reverses its propeller while traveling forward, slowing or stopping the vessel. This results in unpredictable forces and moments that decrease control and maneuverability. This project utilized computational fluid dynamics (CFD) to model the fluid flow during crashback in hopes of determining the physical causes of the unsteady forces and moments that occur. At the Naval Surface Warfare Center in Carderock, MD, there are two CFD approaches being applied to crashback: a pure Large Eddy Simulation (LES) technique and CRUNCH, which is a hybrid of LES and Reynolds Averaged Navier-Stokes (RANS). The LES approach provides extremely detailed three-dimensional, transient turbulence results but, for now, is limited to an open propeller. CRUNCH can also provide turbulent flow data, but it can be applied to more complex geometries, such as a duct or submarine hull. For this research, results generated with the pure LES technique were utilized due to complications that arose from adapting the CRUNCH model to crashback. There were two distinct aspects to this research. First, the LES results were validated against data from experiments with similar advance ratios (a dimensionless parameter relating propeller rotational speed with axial flow velocity). Mean, root mean square, and standard deviation values of the thrust, torque, and side force from the LES code were compared with those from the experiments to ensure the magnitudes and variations in the resultant loads were similar to experimental data. Spectral analysis was also performed on the thrust, torque, and side force magnitudes and angle to determine whether the resultant oscillation frequencies of the LES results were comparable to the response frequencies found in the experimental data. Once the LES results were shown to be sufficiently accurate, analysis was performed to determine

| 14. SUBJECT TERMS | 15. NUMBER OF PAGES |
|---|---|
| Crashback, Computational Fluid dynamics, CFD, Propeller, Submarine | **67** |
| | 16. PRICE CODE |

| 17. SECURITY CLASSIFICATION OF REPORT | 18. SECURITY CLASSIFICATION OF THIS PAGE | 19. SECURITY CLASSIFICATION OF ABSTRACT | 20. LIMITATION OF ABSTRACT |
|---|---|---|---|
| | | | |

# REPORT DOCUMENTATION PAGE

**Form Approved**
**OMB No. 074-0188**



| 1. AGENCY USE ONLY (Leave blank) | 2. REPORT DATE | 3. REPORT TYPE AND DATE COVERED |
|---|---|---|
| | 4 May 2007 | |

**4. TITLE AND SUBTITLE**
Simulation and Evaluation of Marine Propeller Crashback Through Computational Fluid Dynamics

**5. FUNDING NUMBERS**

**6. AUTHOR(S)**
**Shearer, Matthew P.**

| 7. PERFORMING ORGANIZATION NAME(S) AND ADDRESS(ES) | | 8. PERFORMING ORGANIZATION REPORT NUMBER |
|---|---|---|
| | | |

| 9. SPONSORING/MONITORING AGENCY NAME(S) AND ADDRESS(ES) | | 10. SPONSORING/MONITORING AGENCY REPORT NUMBER |
|---|---|---|
| **US Naval Academy<br>Annapolis, MD 21402** | | **Trident Scholar project report no. 358 (2007)** |

**11. SUPPLEMENTARY NOTES**

| 12a. DISTRIBUTION/AVAILABILITY STATEMENT | 12b. DISTRIBUTION CODE |
|---|---|
| **This document has been approved for public release; its distribution is UNLIMITED.** | |

**13. ABSTRACT** (cont.)the physical cause of the unsteady forces. Several sets of animations were created which enabled many different aspects of the flow to be observed simultaneously. These animations were created for forty revolutions, spanning nearly 3.5 seconds. These animations yielded a wealth of insight into the flow field generated by crashback. They showed many different aspects of the flow field that have never been seen before, illustrating the relationships between flow field characteristics and measurable quantities, such as side force. Several theories proposed by other crashback research, such as the influence of the ring vortex, were evaluated through the visualization analysis. First, animations were created by taking constant radial cuts of all five propeller blades, displaying blade cross sections and visualizing the flow field over all the blades simultaneously. The observations provided by these animations prompted the creation of animations that displayed both the location of vortices within the flow (including the ring vortex) and the pressure distribution over the blade surfaces. These two animations did not reveal any direct relationship between vortex locations (including the ring vortex) or the instantaneous pressure distribution and the side force. There was, however, a strong relationship between the pressure fluctuations on the blade surfaces, particularly near the blade roots, and the side force direction. There is no known cause for these fluctuations at this time, but it is theorized that they are due to vortices either ingested into the propeller plane or generated near the blade root, as suggested by the blade sections animations. This research should provide a strong foundation in the computational modeling of crashback.

| 14. SUBJECT TERMS | 15. NUMBER OF PAGES |
|---|---|
| Crashback, Computational Fluid dynamics, CFD, Propeller, Submarine | **67** |
| | 16. PRICE CODE |

| 17. SECURITY CLASSIFICATION OF REPORT | 18. SECURITY CLASSIFICATION OF THIS PAGE | 19. SECURITY CLASSIFICATION OF ABSTRACT | 20. LIMITATION OF ABSTRACT |
|---|---|---|---|
| | | | |

U.S.N.A ---Trident Scholar project report; no. 358 (2007)

# Simulation and Evaluation of Marine Propeller Crashback Through Computational Fluid Dynamics

by

Midshipman 1/C Matthew P. Shearer
United States Naval Academy
Annapolis, Maryland

_____
(signature)

Certification of Advisor Approval

Professor Gabriel N. Karpouzian
Aerospace Engineering Department

_____
(signature)

_____
(date)

CDR Jeffery W. Stettler, USN
Naval Architecture and Ocean Engineering Department

_____
(signature)

_____
(date)

Acceptance for the Trident Scholar Committee

Professor Joyce E. Shade
Deputy Director of Research & Scholarship

_____
(signature)

_____
(date)

USNA-1531-2

# ACKNOWLEDGEMENTS

This research would not have been possible without the help and assistance of many people. First, I would like to thank my advisors, Dr. Peter Chang, Professor Gabriel Karpouzian, and CDR Jeffery Stettler, for their constant support and encouragement throughout the project. There were more than a few times when I was frustrated and upset that things were not working as they should or as I had planned, but they were always there to remind me that research does not always work out the way it was designed. For that, I am deeply thankful. Next I would like to thank the staff at the Naval Surface Warfare Center- Carderock Division for their help. They provided me with more data than I ever thought I could analyze and then helped me sort through it to find what I needed. In particular, I would like to thank Michael Ebert for providing me with the simulation results and aiding me in visualizing them. Also, I want to thank Martin Donnelly, David Fry, and Stuart Jessup, who provided me with the experimental data used for this research. It was a great opportunity to work with the men responsible for many of the papers I read in preparation for this project. I would be remiss if I did not thank the Naval Academy's Computer Aided Design- Integrated Graphics staff for helping me install and set up the software I used for analysis and Multimedia Support Center for helping me prepare my poster and presentation for the Trident Scholar Conference. I would like to thank the Trident Scholar Committee and the Office of Naval Research for providing me with this tremendous opportunity. This project has helped prepare me for future research opportunities, and I am looking forward utilizing the skills I have learned. Finally, I would like to thank my family and friends for their constant support. My parents instilled in me at an early age a respect and desire for knowledge, and they have encouraged me throughout my education. My friends have always been my biggest competition, academically and otherwise, which has motivated me to strive for perfection. There are countless others that have helped along the way, but it is impossible to name them all. Please know that will never forget the contributions everyone has made to this research and my life, and I am forever indebted to each and every one of you.

# ABSTRACT

Crashback is a maneuver which occurs when a ship or submarine reverses its propeller while traveling forward, slowing or stopping the vessel. This results in unpredictable forces and moments that decrease control and maneuverability. This project utilized computational fluid dynamics (CFD) to model the fluid flow during crashback in hopes of determining the physical causes of the unsteady forces and moments that occur. At the Naval Surface Warfare Center in Carderock, MD, there are two CFD approaches being applied to crashback: a pure Large Eddy Simulation (LES) technique and CRUNCH, which is a hybrid of LES and Reynolds Averaged Navier-Stokes (RANS). The LES approach provides extremely detailed three-dimensional, transient turbulence results but, for now, is limited to an open propeller. CRUNCH can also provide turbulent flow data, but it can be applied to more complex geometries, such as a duct or submarine hull. For this research, results generated with the pure LES technique were utilized due to complications that arose from adapting the CRUNCH model to crashback.

There were two distinct aspects to this research. First, the LES results were validated against data from experiments with similar advance ratios (a dimensionless parameter relating propeller rotational speed with axial flow velocity). Mean, root mean square, and standard deviation values of the thrust, torque, and side force from the LES code were compared with those from the experiments to ensure the magnitudes and variations in the resultant loads were similar to experimental data. Spectral analysis was also performed on the thrust, torque, and side force magnitudes and angle to determine whether the resultant oscillation frequencies of the LES results were comparable to the response frequencies found in the experimental data. Once the LES results were shown to be sufficiently accurate, analysis was performed to determine the physical cause of the unsteady forces. Several sets of animations were created which enabled many different aspects of the flow to be observed simultaneously. These animations were created for forty revolutions, spanning nearly 3.5 seconds. These animations yielded a wealth of insight into the flow field generated by crashback. They showed many different aspects of the flow field that have never been seen before, illustrating the relationships between flow field characteristics and measurable quantities, such as side force.

Several theories proposed by other crashback research, such as the influence of the ring vortex, were evaluated through the visualization analysis. First, animations were created by taking constant radial cuts of all five propeller blades, displaying blade cross sections and visualizing the flow field over all the blades simultaneously. The observations provided by these animations prompted the creation of animations that displayed both the location of vortices within the flow (including the ring vortex) and the pressure distribution over the blade surfaces. These two animations did not reveal any direct relationship between vortex locations (including the ring vortex) or the instantaneous pressure distribution and the side force. There was, however, a strong relationship between the pressure fluctuations on the blade surfaces, particularly near the blade roots, and the side force direction. There is no known cause for these fluctuations at this time, but it is theorized that they are due to vortices either ingested into the propeller plane or generated near the blade root, as suggested by the blade sections animations. This research should provide a strong foundation in the computational modeling of crashback.

Key Words: Crashback, Computational Fluid Dynamics, CFD, Propeller, Submarine

# TABLE OF CONTENTS

# NOMENCLATURE

$\omega$ ..... Angular Velocity (radians per second)
$\rho$ ..... Density
$D$ ..... Propeller Diameter
$F$ ..... Force
$f$ ..... Force/Torque Response Frequency
$I$ ..... Total number of data points in a subset
$i$ ..... Data point subset index
$J$ ..... Advance Ratio
$K_{F_h}$ ..... Side Force Coefficient (horizontal component)
$K_{F_v}$ ..... Side Force Coefficient (vertical component)
$K_{F_{mag}}$ ..... Side Force Magnitude
$K_T$ ..... Thrust Coefficient
$K_Q$ ..... Torque Coefficient
$n$ ..... Angular Velocity (revolutions per second)
$Q$ ..... Torque
$U$ ..... Axial Velocity
$x$ ..... Axial Coordinate (inertial reference frame)
$y$ ..... Horizontal Coordinate (inertial reference frame)
$z$ ..... Vertical Coordinate (inertial reference frame)

# 1 INTRODUCTION

## 1.1 Crashback

Crashback is one of four primary modes of operation for ships and submarines. As shown in Figure 1, crashback occurs when the vessel has positive axial velocity and the propeller has negative angular velocity. In other words, the ship or submarine is moving in the forward direction and reverses its propeller, typically used in slowing or stopping the vessel while underway.

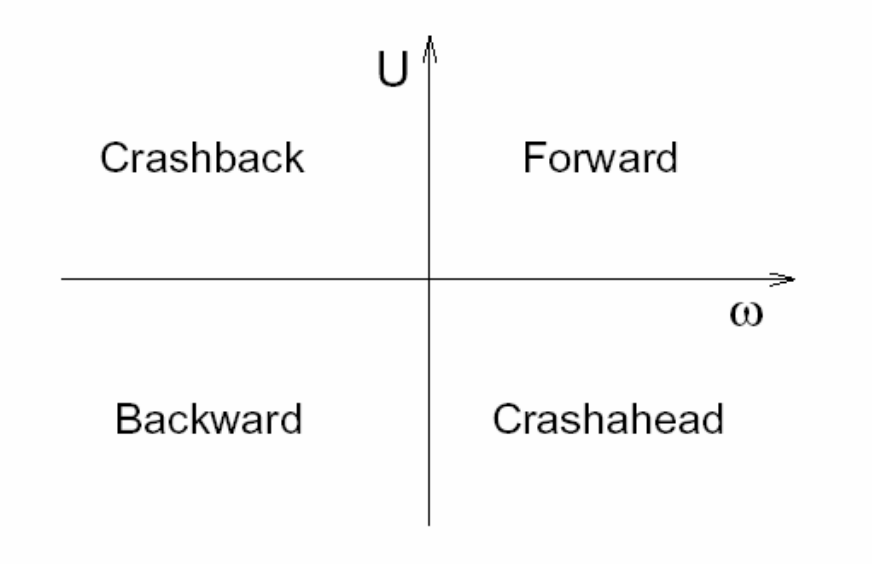


Figure 1- Marine vessel modes of operation in terms of axial velocity ($U$) and propeller angular velocity ($\omega$).

While this may seem like a trivial event that takes place on a routine basis, it is very important in determining the operational envelope of a vessel. Naval vessels are not permitted to operate at a speed any faster than the speed at which they can safely stop.

Crashback, surprisingly, is hardly a routine operational maneuver. During crashback, unsteady forces and moments act on the propulsor and, in turn, the entire vessel, making safe control and maneuvering difficult to impossible, particularly for submarines. These forces and moments tend to result in abnormal behavior in the pitch and yaw of the vessel. This has become a more significant problem lately, as the Navy has begun a shift toward littoral

operations as opposed to open ocean combat. Any uncontrolled pitch of a submarine operating in shallow waters could result in a breach of the surface or contact with the floor, announcing its presence and potentially endangering the boat and crew. Another adverse effect of crashback is unnecessary stress on the propeller blades. The oscillation of the forces and moments during crashback cause propeller blades to wear more quickly than normal operation. The more that is understood about these forces and moments, the more effectively they can be managed and the better the operational envelope can be.

One theory regarding the source of the unsteady nature of the forces and moments has to do with a fluid structure known as the vortex ring. The difference between the negative axial velocity near the center of the propeller, caused by its negative rotation, and the positive axial velocity that occurs near the blade tips, due to the forward motion of the vessel, results in a circulation that takes the form of a torus near the tips of the propeller blades. Jessup *et al*. (2006) documented the existence of the vortex ring using Particle Image Velocimetry (PIV) and Laser Doppler Velocimetry (LDV) data taken in the 36" Variable Pressure Water Tunnel (VPWT) at the Naval Surface Warfare Center in Carderock, MD (NSWCCD) in 2004. This fluid structure can be created by ejecting a cylindrical volume of fluid rapidly through a cylindrical tube; however, there is a major difference between the vortex ring created by a fluid pulse and the one formed during crashback. The fluid pulse vortex ring is stable, because it has no rotational component. The rotation of the propeller causes the vortex ring to rotate as well, as shown by Stettler (2004). Some believe that the oscillation of the forces and moments is due to the formation and breakup, or shedding, of the vortex ring during crashback, as presented by Višohlíd and Mahesh (2006). Another belief is that the vortex ring forms asymmetrically, resulting in a force acting on the propeller, and rotates, causing the oscillation of that force, demonstrated by Bridges *et al*. (2005). These theories could potentially provide insight into the crashback phenomenon, but experimental data do not provide the required information for the types of analysis necessary to evaluate them.

## 1.2 Computational Fluid Dynamics

Many experiments have been performed over the years in hopes of determining the origins of the forces and moments that act on the propulsor during crashback. Experimental tests allow data to be collected from vessels, models, or propulsors operating in crashback; however, these data can only be recorded for a small portion of the experimental domain. For example, experimentalists are able to obtain time-series velocity data, both magnitude and three-dimensional direction, over the course of an experiment using techniques such as PIV and LDV. PIV data can only be captured for a single, two-dimensional plane within the system, and LDV data can only be recorded for a single point at a time. While these experiments have produced a wealth of excellent data, it is very difficult to use these data to extract the physical cause of the forces and moments that occur during crashback. With regard to vortex rings, it is difficult to determine their magnitude, shape, location, and rotational speed all at once. While experimental data have shown evidence of their existence, two-dimensional representations of them do not provide enough information to perform proper analysis. In essence, while experimental data are relatively easy to obtain, the data are not sufficient to provide the insight necessary to evaluate a complex phenomenon such as crashback. For this reason, computational fluid dynamics (CFD) has been called upon to provide a more accurate picture of what goes on during crashback. Computational methods of analysis have been shown in other engineering fields to be invaluable in evaluating complex systems, and they promise to have the same effects in analyzing crashback.

The governing equations of fluid dynamics are the Navier-Stokes equations, and they are based on the principles of conservation of energy, mass, and momentum. When this system of equations is solved, a unique pressure and velocity field can be obtained for any Newtonian fluid system, in which the stress-strain rate relations are linear. There are analytical solutions for simple flow fields, but they simply do not exist for complex flow fields, such as those that exist during crashback. Computational methods must be utilized to obtain the pressure and velocity fields. Computational fluid dynamics essentially solves the Navier-Stokes equations at every point in a computer generated grid system to obtain three-dimensional pressure and velocity fields. These three-dimensional flow fields provide an opportunity to observe the entire vortex

ring at once. These fields can also be used to calculate characteristic values, such as vorticity, within the vortex ring, or they can be animated to create visualizations of the vortex ring formation and shedding. The CFD results provide nearly endless possibilities for analysis and evaluation and can hopefully lead to explanations of the crashback phenomenon.

### *1.2.1 LES and RANS*

There are many different techniques that fall under the category of computational fluid dynamics. Reynolds-Averaged Navier Stokes equations (RANS) and Large Eddy Simulations (LES) are currently two of the most prominent CFD techniques. RANS codes are excellent at evaluating flows fields that involve attached, turbulent flow, but they utilize a momentum dissipation mechanism that is used to mimic the effects of turbulent flow. This dissipation mechanism is able to simulate large scale separation in complex systems like crashback, but smaller, more random scales are dissipated. RANS turbulence models must resolve turbulence on all scales, which is often extremely complex and unreliable for complicated flows such as crashback. The scales of the flow fluctuations in crashback demand that the computational codes be able to dependably model turbulence at these small scales.

LES codes provide more accurate modeling of separated flow fields than RANS models, a result of the code being based on energy-conserving turbulence models. The LES code models the “energy-containing” turbulence scales, and uses a “sub-grid scale” to model smaller scale turbulence. Turbulence on these scales can be assumed to be isotropic, so they can be modeled more simply than those in the RANS simulations. In order to resolve turbulence on these scales, the LES codes must have very strict time step and grid size requirements, making them much more computationally intensive than RANS codes.

### *1.2.2 CRUNCH*

While LES codes are better able to model small-scale turbulence than RANS codes, RANS codes are much more efficient in regions where the flow is attached. A company named CraftTech, Inc. has developed a code which applies the relative advantages of both RANS and LES codes to achieve a highly efficient and accurate computational model for all regions of the

crashback system. CRUNCH utilizes RANS modeling on the pressure side of the propeller blades and in attached flow regions and LES modeling in regions where the flow has become separated. This allows accurate results to be obtained for the separated regions while reducing computing time. The RANS modeling still provides good results in the attached flow region but does not adversely affect the results in the separated flow region. The LES modeling in the separated flow regions yields accurate results, but the computing time is not increased any more than necessary because it is not used throughout the entire system. This hybrid has the potential to yield accurate results without unnecessary computational time.

### *1.2.3 LES Model*

Unfortunately, there were issues adapting CRUNCH to model crashback which prevented the research from being performed using this particular CFD technique. Instead of evaluating CRUNCH, as intended, the same validation and analysis were performed using an LES code developed at the University of Minnesota and provided by Dr. Krishnan Mahesh. The code was transitioned to NSWCCD, where simulations were run by Michael P. Ebert. Simulations were performed at NSWCCD on a P4381 propeller, for which experimental data exist for use in validation. Propeller 4381 is a right-handed propeller with five variable-pitch blades with no rake or skew and a diameter of 12 inches (details can be found in Jessup et al, 2004). Rake is defined as the amount that propeller blades are slanted aft of a plane perpendicular to the shaft axis, and skew is the amount that blades are swept back from the direction of rotation (a radially symmetric propeller has zero skew). The CFD control volume, shown in Figure 2, consists of a cylinder with a radius equal to 7.3 times the propeller diameter, corresponding to the maximum radius of the VPWT in which the propeller was tested. The length of the control volume is equal to 13.75 times the propeller diameter. The grid used for this research was composed of approximately 13 million control volumes and was created using a commercial grid generator known as Gambit and TGrid (Fluent Corporation). The grid utilized four layers of prism elements growing out from the blades surfaces, transitioning into tetrahedral elements near the blades to accommodate the complex geometries of the blades themselves. The grid uses hexahedral elements in the outer regions to increase efficiency. The four layers of prisms grown

on the blade surfaces improve the accuracy in modeling boundary layers on the blades. This particular LES model utilizes a dynamic Smagnorinsky sub-grid model, which calculates the turbulent momentum flux due to unresolved turbulence scales based upon the strain rate of the smallest resolved turbulence scales. The LES code solves the Navier-Stokes equations in a rotating frame of reference, such that the propeller geometry is stationary and the flow rotates about it. In order to accomplish this, the propeller remained stationary, and a rotational component was added to the inflow velocity to simulate the propeller motion. The flow at the surfaces of the blades, hub and shaft was set to the rotational speed at that radius (no-slip boundary). A constant free-stream velocity boundary condition is applied at the inflow and lateral boundaries while a convective velocity boundary condition (stream-wise derivatives are required to be zero) is set at the outflow boundary (Višohlíd and Mahesh, 2006).

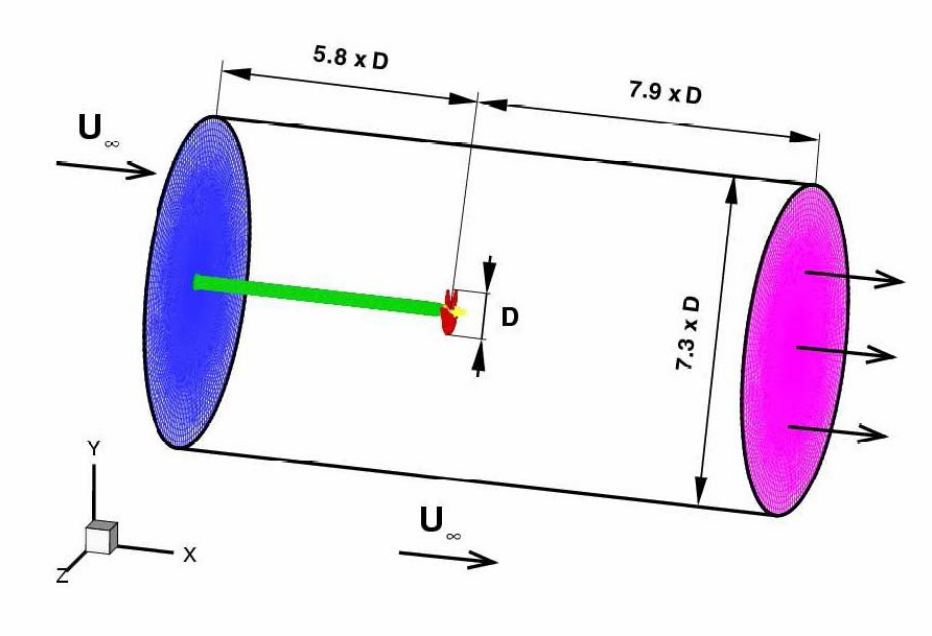


Figure 2- Control volume simulated by CFD code.

## 1.3 Research

The purpose of this research is twofold: to validate the computational results from the LES code and to evaluate the flow field to determine possible origins of the unsteady forces and

moments. First, in order to evaluate the validity of the CFD technique, the computed results for the thrust, side force, and torque acting on the propeller were compared with the data recorded in experimental tests. The unsteady nature of the forces and moments requires that spectral analysis be performed to determine whether the frequency of the force and moment oscillations were similar to those found in the experiments. Once these characteristics are compared and found to be in agreement, then analysis of the flow field itself can begin. One of the disadvantages of experimental data is that it can only be taken for limited portions of the control volume. By utilizing CFD codes, the pressure and velocity field can be calculated for every point within the system. These values can be used to calculate other parameters, such as vorticity and forces, which can then be displayed and animated in three dimensions. Looking at the flow field and its properties in three dimensions may help reveal the sources of the unsteady forces and moments that occur during crashback.

This research is merely the first step in an extensive effort of computational analysis of crashback. Once the computational code and model establishes that it can accurately represent the flow field during crashback, the system will increase in complexity until it can eventually model an entire ship or submarine operating in dynamic crashback. The ultimate goal of crashback research is to develop new technologies, equipment, and/or procedures that will improve vessel operation in crashback. This will not only improve the operational envelope of the vessel, it will also improve the safety of the vessel and crew. Computational methods will allow for the analysis of complex systems like crashback without the time-consuming process of constructing physical models or the expensive operation of testing facilities. The computational process is costly and time-intensive now, but it will prove to be a valuable technique once it is proven accurate.

# 2 VALIDATION

## 2.1 Procedure

### *2.1.1 Experimental Setup and Data Reduction*

One of the main purposes of this research is to help validate the results of computational approaches to the crashback problem. To facilitate this process, force and moment values were obtained from both experimental data and CFD calculations that could be easily compared to determine if the computational process produced valid results. These values include the side force (components, magnitude, and direction), thrust, and torque acting on the propeller during crashback. These are typical parameters evaluated by experiment, so they will be useful in validating the computational results. Data were obtained for nearly 120 experimental test runs performed in the 36" VPWT at NSWCCD and over 130 test runs performed in the Large Cavitation Channel (LCC) in Memphis, Tennessee at a wide range of axial velocities and propeller speeds. One of the performance parameters of propeller operation is the advance ratio, $J$, which is simply a measure of the axial velocity of the flow, $U$, normalized by the product of the rotational velocity of the propeller, $n$, in revolutions per second and the diameter of the propeller, $D$.

$$J = \frac{U}{nD} \tag{2.1}$$

The advance ratio is a kinematic similarity parameter that is proportional to the ratio of the axial velocity to the tangential velocity at any point on the propeller. Its use allows tests performed at varying velocities and rotational speeds to be compared, regardless of scale. The local Reynolds number based on the chord and velocities at the 0.7 radius for J=-0.5 is approximately 2 million, indicating that the flow over the blades can be assumed to be turbulent. The Reynolds number is flow parameter that is defined as the ratio of inertial to viscous forces (Equation 2.2), and it is used to compare flows that occur on different length scales. It is typically calculated based on the propeller diameter, $D$, the axial flow velocity, $U$, and the kinematic viscosity of the fluid, $\nu$, as shown in Equation 2.2. Sometimes in flows such as crashback the velocity and

characteristic length are taken at specific regions of the flow, as mentioned above, to obtain a local Reynolds number to get a better idea of the nature of the flow in that specific region.

$$\mathrm{Re} = \frac{DU}{\nu} \qquad 2.2$$

In the VPWT experiments, force and torque measurements were recorded for a P4381 mounted on a shaft. In order to properly simulate these conditions, the CFD code used the model shown in Figure 2. The LCC tests were performed with a P4381 mounted on a scale submarine hull, so it is a completely different test setup than what is being evaluated using the LES code. Currently, this setup is too complex to model using LES, but the results of this study could lead to the development of this capability in the future. Currently, the only available LES results are for advance ratios of -0.3, -0.5, and -0.7. The same analysis was performed on all the experimental data (both the VPWT and LCC tests). The LES results chosen for this research have an advance ration of -0.5, so only the experimental data with similar advance ratios were used for validation. The two most relevant test runs were Run 174 and Run 187 performed in the VPWT, and their experimental conditions are compared to those simulated by the LES model in Table 1.

Table 1- Experimental conditions for VPWT tests compared with simulated conditions for LES modeling.

| | U (ft//s) | RPM | J |
|---|---|---|---|
| 174 | 5.926406 | -699.874 | -0.50807 |
| 187 | 5.879681 | -700.218 | -0.50382 |
| LES | 5.833333 | -700 | -0.5 |

Initially, it was proposed to evaluate the new CRUNCH CFD code, developed by CraftTech Inc., because it is a hybrid that combines two different CFD techniques, LES and RANS. The CRUNCH code represents the latest technology in CFD and has the potential to be a more effective computational tool for the evaluation of crashback. Unfortunately the code has taken longer to adapt to the Crashback scenario than expected. There were issues regarding boundary conditions, grid sizing, and momentum conservation that resulted in unusable results.

The same data analysis procedure that was to be utilized for the CRUNCH results was performed on both experimental data and computational results obtained from the LES code. While the current data analysis applies to an LES model, the principle has not changed. The LES results must be validated against the experimental data, just like the CRUNCH results. These results could prove invaluable to the study of crashback, and they can only serve to improve the quality of the research. Initial CRUNCH results should be available in the near future, and the results of this research will help guide that analysis.

The VPWT data used in this evaluation have been reduced to negate as many non-hydrodynamic effects as possible. Data were taken to record the weight of the propeller at various angles of orientation, so that it could be subtracted from the results. This was necessary to remove the effects of any weight imbalances in the propeller that occurred during construction, which would present themselves as components of the side force in the recorded data. The side force data were measured in the rotating (propeller) reference frame, but were converted to the inertial reference frame for analysis. The LES code being evaluated modeled a stationary propeller and used rotating flow in order to simulate propeller rotation, but the side force results were recorded in the inertial frame of reference, so no conversion was necessary. The force and moment values from both the experiment and LES code were then normalized into force and torque coefficients, defined as:

$$K_F = \frac{F}{\rho n^2 D^4} \tag{2.3}$$

$$K_Q = \frac{Q}{\rho n^2 D^5} \tag{2.4}$$

This is the standard normalization used in propulsion experiments and, therefore, the results can be used to compare with standard propulsion test data.

### *2.1.2 Spectral Analysis*

Due to the unsteady nature of the crashback phenomenon, Fourier analysis was performed on the experimental data to determine the frequency at which the resultant loads act on the propulsor. Fast Fourier Transforms (FFT) were performed on two experimental runs and

the computational results using the Data Analysis Toolpak add-in available in Microsoft Excel. Other software, such as MATLAB, would be better suited for the spectral analysis performed on these datasets, but it was not readily available during a large portion of this research. The small increase in the quality of the spectral analysis for this research did not justify the time required to rewrite the automated system used in order to reproduce these results once MATLAB became available. The FFT program used limited the number of data points in each subset to 4096, even though the time series datasets are comprised of over 30,000 points. This demanded that the operations be performed on multiple subsets within each run of data. The advantage of breaking the long time series into smaller realizations is that the amplitude spectra from each realization could be averaged together, resulting in smoother results. Also, the vast majority of the time series data is accounted for rather than leaving off significant portions of the beginning and end of the run. The disadvantage of the relatively short realizations is that the lower frequencies are not well-resolved. The mean of the entire run was subtracted from each time series value to minimize the effect of the magnitude of the data on the results. Despite the limitations of this particular FFT program, the spectral analysis was accurate enough to demonstrate the LES code's ability to properly model the force, torque, and angle response frequencies present in the experimental data.

A Hanning Window (Equation 2.5) was applied to each set to reduce the error inherent in obtaining frequency results for data with nonzero endpoints. In order to reduce what is known as ringing, which occurs when the Fourier analysis is used to approximate a step input, the Hanning Window sets the endpoints of each subset to zero. Figure 3 shows the effect of the Hanning Window equation on the data. It is clear how the Hanning Window smoothly limits the data to zero at both endpoints of each dataset. To compensate for the disparity in magnitude between the original data and the Hanning Window, the root mean square (RMS) value of the original data set and the data in the Hanning Window were calculated. The values in the Hanning Window were multiplied by the ratio to ensure that the total energy in the final data set was the same as the original. Finally, to ensure that all the data were properly accounted for, each time an FFT was performed, the data were offset by half of the previous data set, allowing the data points that were minimized due to the low magnitude at the ends of each Hanning Window to be utilized. This resulted in 13 subsets, over which the FFT results were averaged.

$$w(i) = \frac{1}{2}\left(1 - \cos\left(\frac{2\pi i}{I-1}\right)\right) \qquad 2.5$$

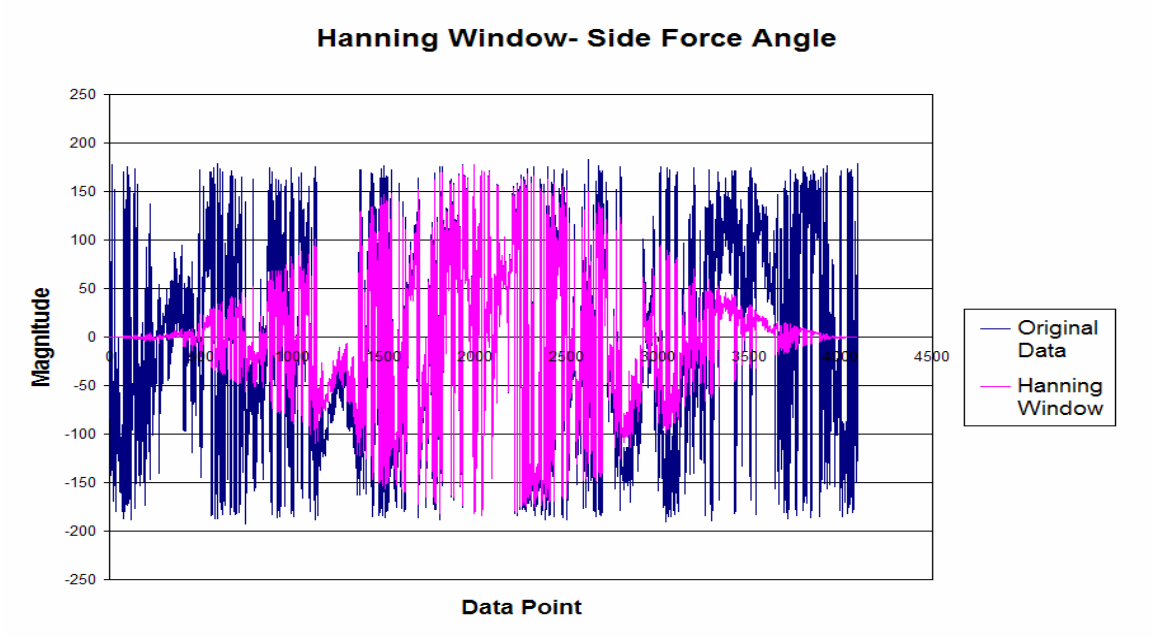


Figure 3- Hanning Window applied to data set.

The output of the FFT was a complex number corresponding to the Fourier coefficient multiplied by the number of values in the subset. In order to obtain the magnitude of the spectral response at a given frequency, the magnitude of the complex Fourier coefficient was calculated and divided by the number of data points in the subset, which, in this case, was 4096. The data from each subset were then averaged and converted to decibel values to facilitate the comparison of large range of magnitudes within the same spectra. The frequency corresponding to each coefficient was calculated by dividing the number corresponding to the result, 0 through 2048 (the output is symmetrical, and the highest frequency that can be resolved is half of the sample rate; only the first half is applicable), by the total time represented by the original dataset. This frequency is represented as a factor of the shaft rate. In other words, a response that occurs once per revolution is represented at a frequency of 1.0 (or $10^0$). This allows experiments that occur at varying shaft rates to be compared directly, rather than needing a conversion to account for the different angular velocities. The frequency values were plotted on a logarithmic scale, because the focus of this study is the low frequency response. High frequencies result in vibrations that

may affect the structural integrity of the propulsor, but the low frequencies are the focus of this research. It is oscillations in this region that are responsible for the control difficulties that occur during crashback.

As previously mentioned, the spectral analysis portion of the research was performed on two of the experimental test runs. Runs 174 and 187 were chosen, because they had advance ratios very close to -0.5 (Table 1) and they had lower sampling rates than the other tests performed at $J = -0.5$. The lower sampling rate (500 Hz) resulted in the 30,000 data points within each dataset spanning approximately 60 seconds of testing. During each of these tests, the propeller rotated approximately 700 times, as the tests were performed at a shaft rate of 700 rpm. The more revolutions available, the better the spectral analysis software is able to resolve low frequency responses. Twelve of the 115 experimental tests performed in the 36" VPWT had an advance ratio within 0.1% of -0.5, but Runs 174 and 187 provided the best data for the spectral analysis.

### *2.1.3 Results*

#### 2.1.3.1 Mean, Standard Deviation, and Root Mean Square Values

In order to validate the CFD results, the mean, root mean square, and standard deviations for the thrust, side force, and torque coefficients were compared with the experimental data from the VPWT. Comparing the mean values of the coefficients helped determine whether the computational results have the same average values as the experimental data. The standard deviation helped determine whether the departure of the computational results from the mean value is similar to that of the experimental data. The root mean square (RMS) values compared the magnitudes of oscillating results rather than their actual (signed) values, negating the effect of negative values and helping to determine whether the magnitudes of the oscillations are comparable between the computational and experimental results. The RMS values were only compared for the side force components, because they were the only quantities that oscillated about zero, resulting in both positive and negative values. Mean, standard deviation, and RMS values for the thrust, side force, and torque coefficients were found for the experimental and

computational runs. The mean values are displayed in Figure 4 and Figure 5, the standard deviation values are displayed in Figure 6, and the RMS values are shown in Figure 7.

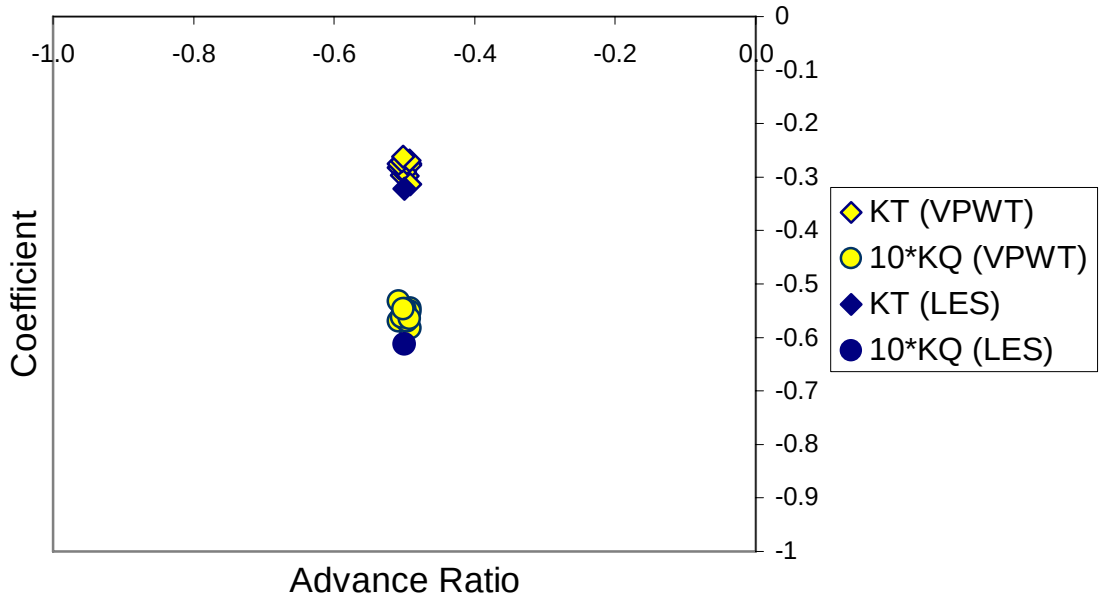


Figure 4- Mean thrust and torque coefficients at $J = -0.5$.

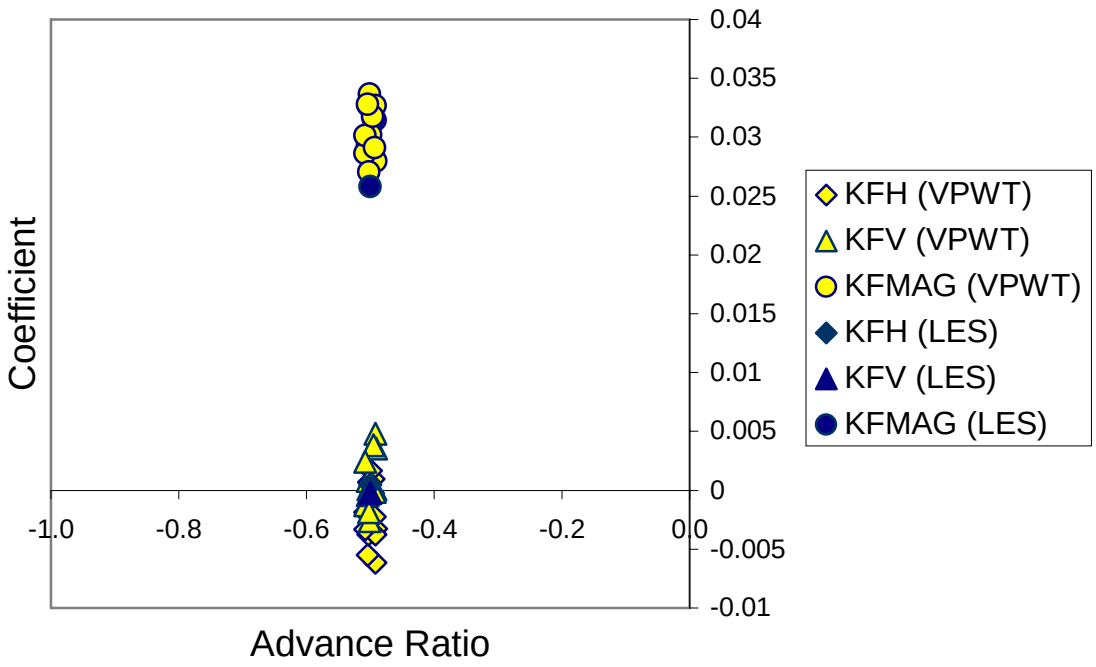


Figure 5- Mean side force coefficients (magnitude and components) at $J = -0.5$.

The results displayed in Figure 4 and Figure 5 clearly show the accuracy of the LES results. The unsteady nature of crashback results in wide scatter in measured quantities among similar tests. The mean values for all the LES quantities displayed lie within these scatters. In particular, the mean side force values lie right in the middle of the scatter from the experimental data. The mean values for the thrust and torque values, while corresponding well with the experimental data, are all toward the lower end of the scatter (higher magnitude). This is likely caused by the effects of cavitation, which decreases the efficiency of the propeller and, thus, the thrust and torque, in experimental testing. While the computed thrust and torque values were greater than the experimental data, the mean side force magnitude is less. This is likely due to having to adjust the dataset to accommodate the spectral analysis code. The sampling rate used during the LES computation was so high that there were not enough revolutions present in the subsets (4096 data points) to produce viable frequency analysis. In order to rectify this, the sampling rate was decreased significantly. This decrease results in some high frequency peaks

being eliminated from the LES results. If these peaks occur between the data points in the adjusted results, then they have no effect on the mean value of the LES results. It is likely that the loss of these peaks could decrease the mean enough that it would lie near the bottom of the scatter. In retrospect, it would have been better to perform the mean, standard deviation and RMS evaluation and the spectral analysis on different sets of LES results (one adjusted and one not), but even with the decreased sample rate, the LES results accurately model the experimental data.

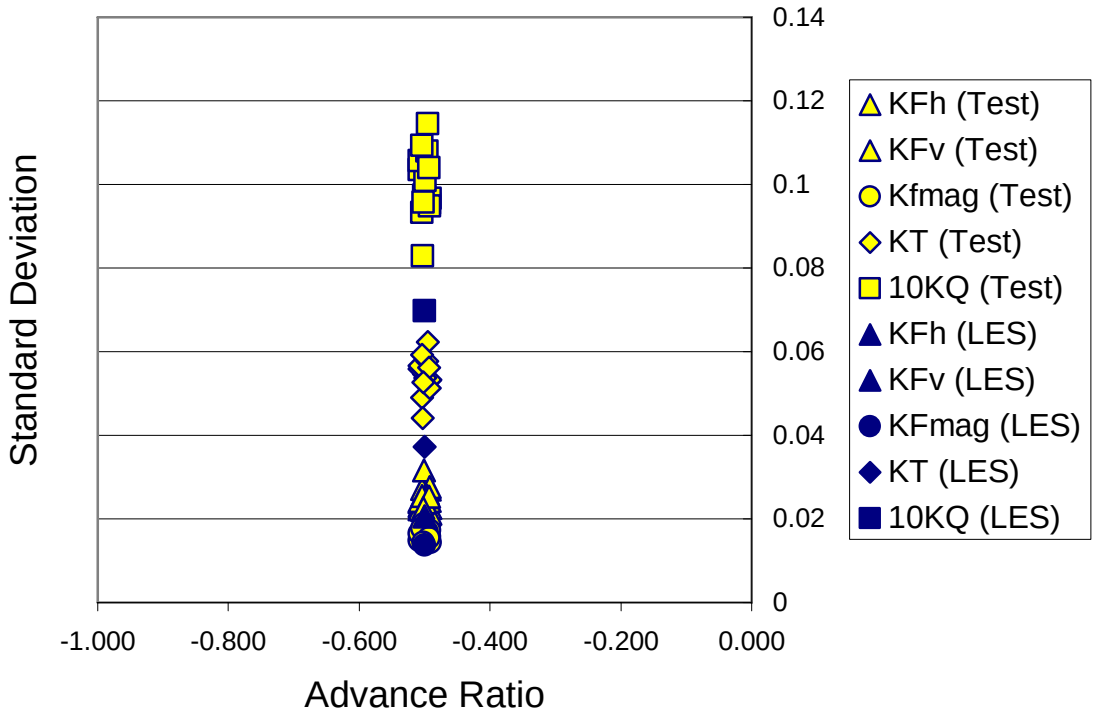


Figure 6- Standard deviation values for the experimental data and LES results at $J = -0.5$.

Figure 6 displays the standard deviation values for the LES results compared with those from the experimental data. The standard deviation values from the LES results tend to be low compared to those for the experimental data, but they still correspond well to their experimental counterparts. This difference is likely due to the influence of cavitation and mechanical vibrations on the recorded experimental data, whereas these were not modeled in the LES code. The cavitation could result in larger oscillations in the experimental data than the LES results.

Similar to the mean values shown previously, there is range of scatter involved with the standard deviation values of the experimental results, which is due to the unsteady nature of the crashback flow field. The standard deviations for the side force quantities (both components and magnitude) lie within this scatter, indicating that the LES code models the side force well. While these values do not correlate quite as well as the mean values, it is clear that this particular model accurately represents the physical tests, especially considering that the model does not include the effects of cavitation and mechanical vibrations.

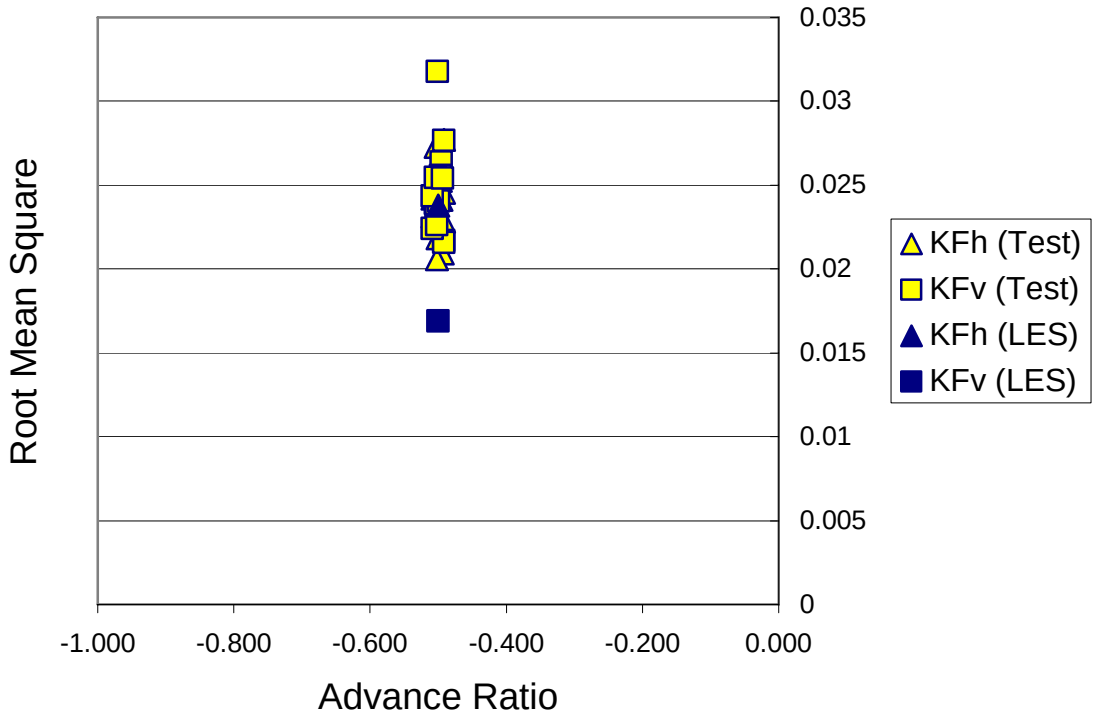


Figure 7- Root mean square values calculated for both experimental data and LES results at $J = -0.5$.

Figure 7 shows the root mean square values for the side force components. The RMS validation was only performed for the side force components, because the oscillations have positive and negative values, whereas the values for thrust and torque are all negative and those for side force magnitude are all positive. The mean values represented earlier indicate that the side force components oscillate around zero, but it gives no indication of whether or not the oscillation magnitudes are similar. The RMS values were taken of the side force components in

order to compare these oscillations. The RMS calculated for the horizontal component of the LES results is located directly in the middle of the scattered experimental data. The RMS value for the vertical LES component seems to be less accurate, but there is also a data point for the experimental data that is similarly removed from the scatter. It must also be taken into consideration that there are only approximately 100 revolutions of the LES simulation computed compared to 700 revolutions for some of the test runs. More LES results will likely improve this accuracy, as will the eventual incorporation of flow characteristics such as cavitation. Regardless of the current limitations of this LES code, it still models the measured force and torque quantities very well.

#### 2.1.3.2 Spectral Analysis

In order to determine whether the frequency responses of the thrust, torque, and side force in the computational results are valid, spectral analysis was performed using Fast Fourier Transforms. The results of the spectral analysis performed on the experimental and computational calculations are shown below in Figures 6-10.

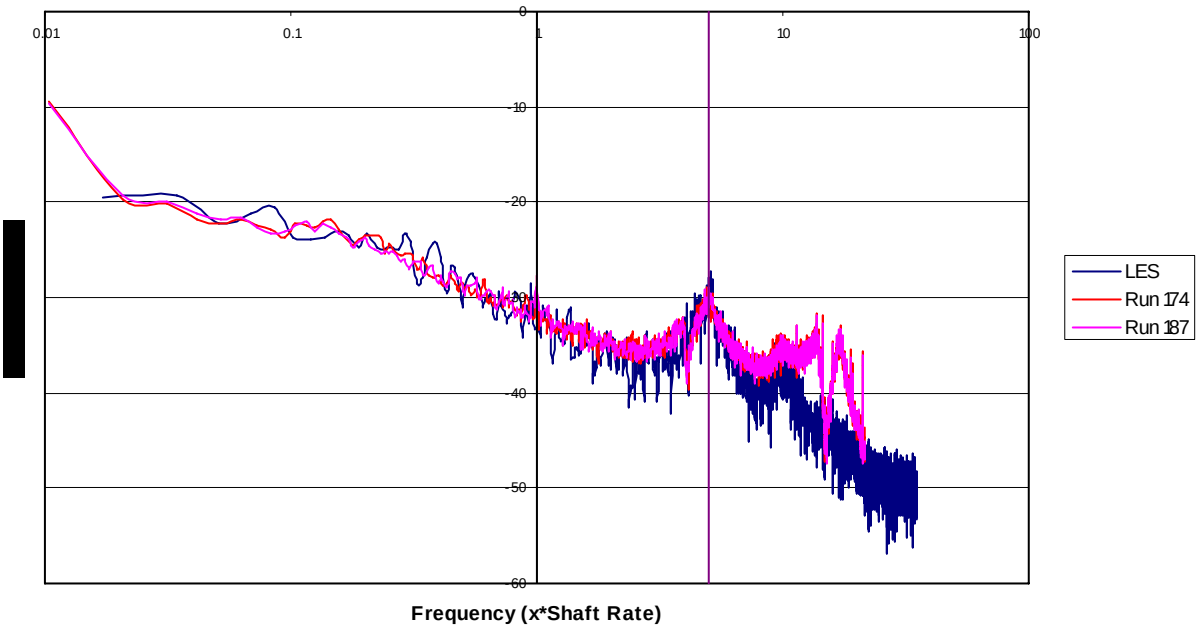


Figure 8- Spectral analysis on thrust coefficient; vertical lines indicate shaft rate and blade rate (5*shaft rate).

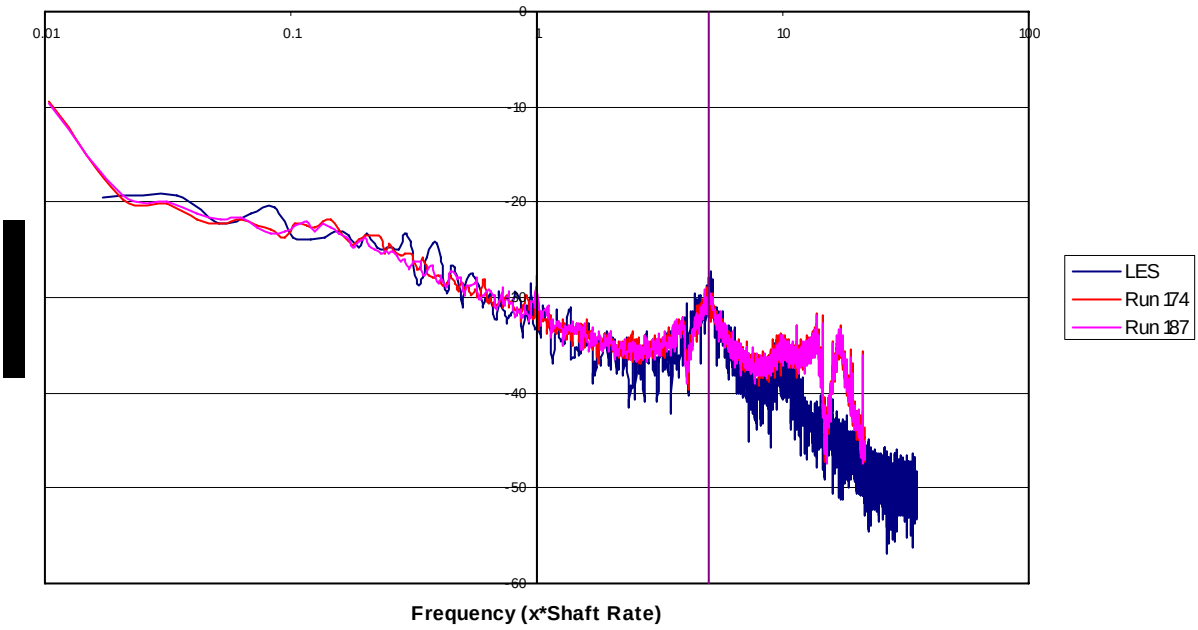


Figure 9- Spectral analysis on torque coefficient; vertical lines indicate shaft rate and blade rate (5*shaft rate).

Figure 8 and Figure 9 display the results of the spectral analysis performed on the thrust and torque coefficient, respectively, for both the experimental and computational data. Clearly, the LES results follow the same low frequency trend as the experimental results, up to the blade rate. First, there are significant drops in energy in the experimental results at 4.0 and 15.0 times the shaft rate, while the LES response is significantly less pronounced at these frequencies. The experimental data also have an energy build-up at frequencies greater than ten times the shaft rate that is not apparent in the CFD results. Like many of the anomalies between the LES results and the experimental data, it is likely that these energy drops are due to physical aspects of the experiment that are not modeled in the LES code. This is particularly likely for these high frequency inconsistencies, as destructive interference from cavitation or mechanical vibrations would result in sharp drops near specific frequencies. Also, as mentioned, many of the high frequency responses were removed from the LES results when the sampling rate was decreased, which would result in lower response magnitudes in the high frequency range. While this appears to be a concern, it is not a significant problem, as the primary focus of this research is

low frequency response. The frequencies of the sharp anomalies are greater than that of the shaft rotation, so they are of little concern to this evaluation of crashback. Second, the lowest frequency for the experimental data appears to be approaching a maximum at a very low frequency; however, there are no data in that frequency range to confirm this. It is caused by the FFT trying to approximate mean values for each subset ( $f = 0$ ). As previously noted, the mean from the entire dataset was subtracted from each term, but the relative mean of each subset was slightly different. Removing this relative difference could have affected the results, so the mean of each subset was not removed. Again, this issue could be resolved by using software better designed to perform this type of analysis. This response is not present in the LES calculations for two reasons. First, the sample rate and dataset size do not support evaluation at frequencies this low. Second, there are only two subsets for each dataset, so the difference in mean value between subsets is minimal. More results are required to perform analysis in this frequency range. Another likely cause is the FFT trying to approximate the Hanning Window. The function used for the Hanning Window has a period that is twice the length of the subset, so the FFT is likely modeling this low frequency. Other than these two issues, the LES calculations model well the corresponding experimental results.

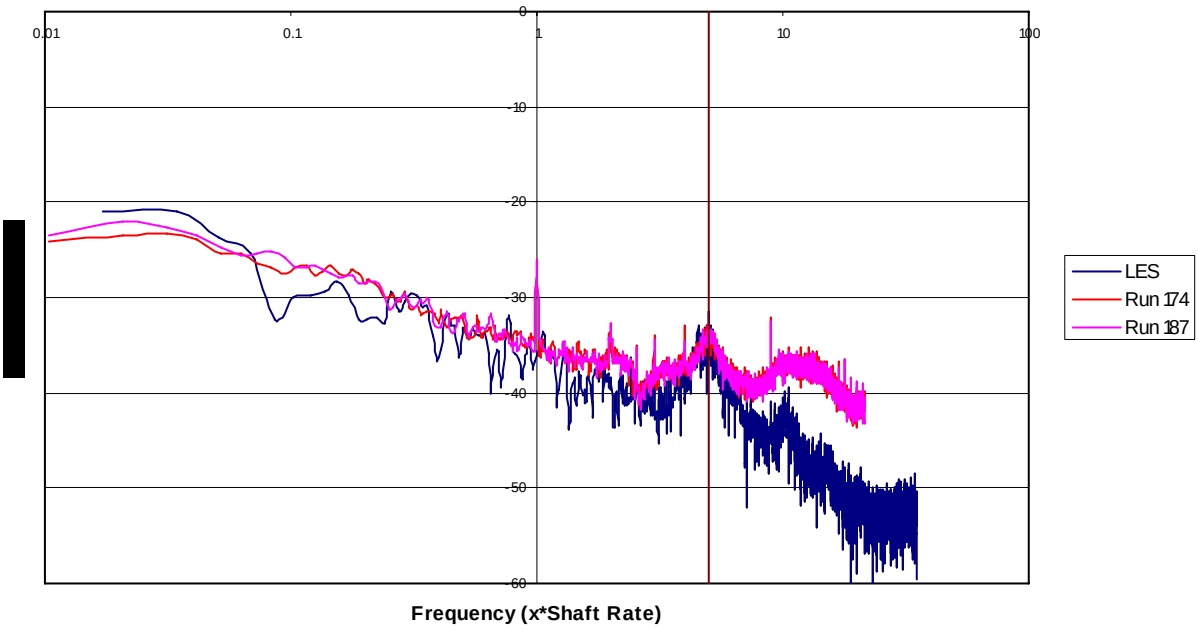


Figure 10- Spectral analysis on horizontal side force coefficient; vertical lines indicate shaft rate and blade rate (5*shaft rate).

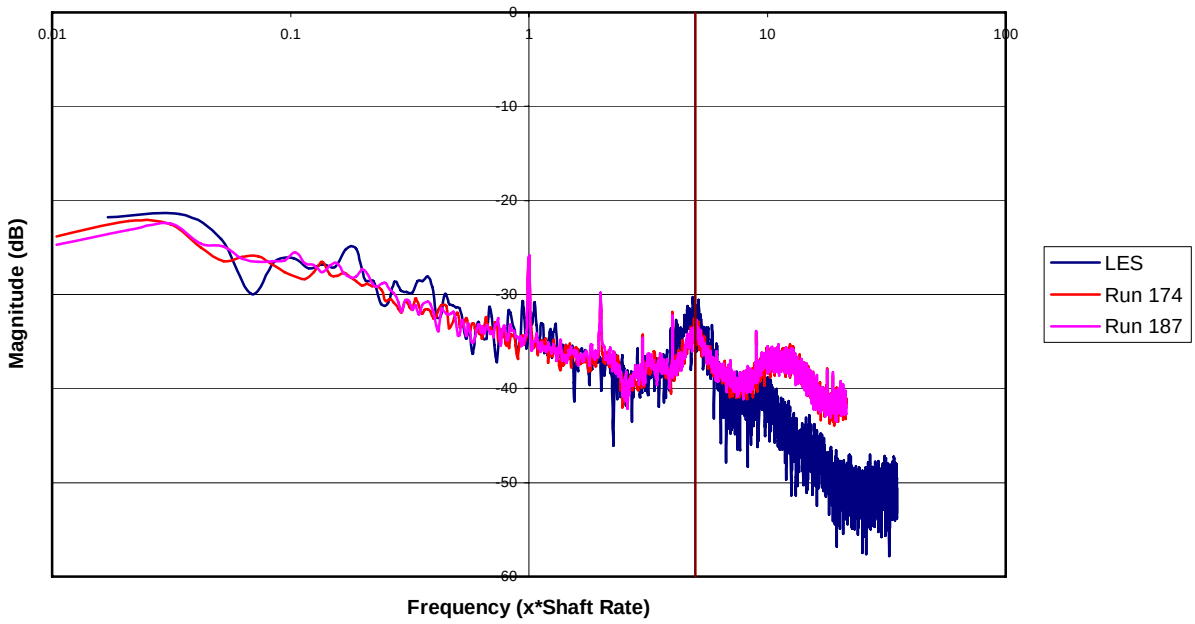


Figure 11- Spectral analysis on vertical side force component; vertical lines indicate shaft rate and blade rate (5*shaft rate).

Figure 10 and Figure 11 show the FFT results of the side force components. As expected, the results of the horizontal and vertical side force components are very similar. These figures show that the horizontal and vertical side forces oscillate at similar frequencies, indicating that the direction of the force rotates in a circular motion around the x-axis. The low-frequency peak for both the experimental and computational results occurs at approximately 0.03-0.05 times the shaft rate, approximately every 20-30 revolutions. This result is even more pronounced in Figure 12, which displays the results of the spectral analysis performed on the side force angle. The LES results also have a similar peak at 5.0 times the shaft rate, the blade rate, similar to the experimental data. There are several peaks at other integer multiples of the shaft rate in the experimental data, but this is simply a function of the propeller weight. As previously mentioned, the propeller weight was subtracted from the recorded data; however, it is nearly impossible to match exactly the propeller angle corresponding to the recorded data and the angle corresponding to the recorded weight, resulting in a residual effect from weight asymmetry

on the experimental force and moment data. The very first set of data used in the spectral analysis included the full propeller weight, and the peaks at the integer multiples of the shaft rate were much more pronounced. The corrected experimental data was obtained, but clearly there are still residual effects from the imbalanced propeller weight.

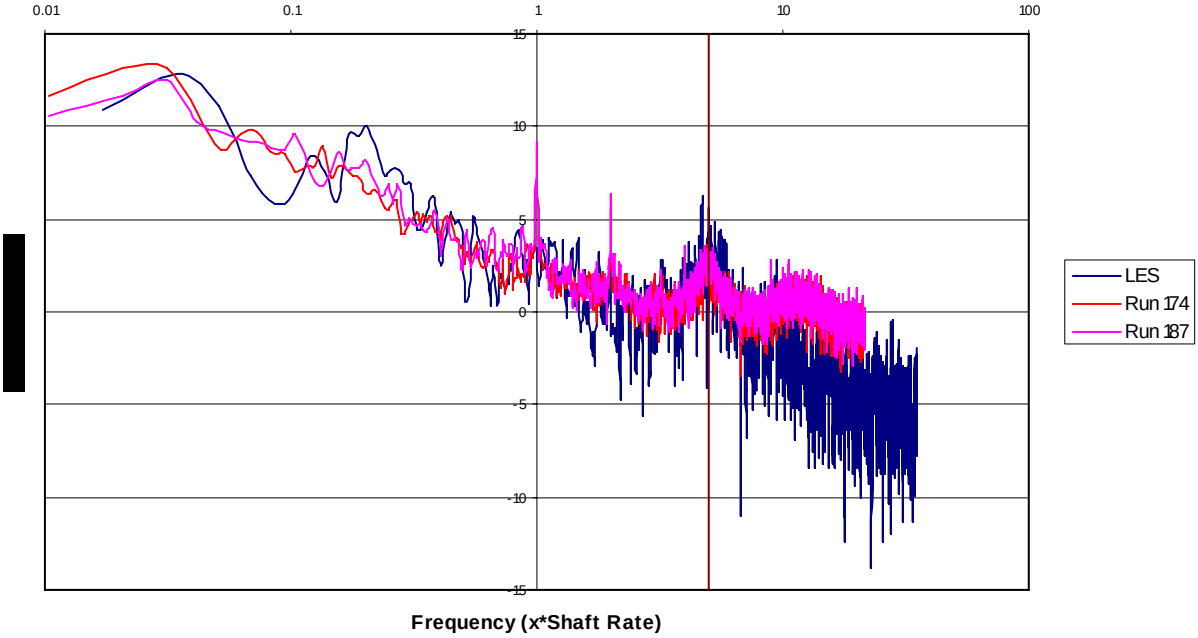


Figure 12- Spectral analysis on side force angle; vertical lines indicate shaft rate and blade rate (5*shaft rate).

In Figure 12, it is clear that there is a significant response in the side force angle that occurs approximately every 20-30 revolutions (i.e. at frequencies between 0.03 and 0.05). The large peak in both the horizontal and vertical side force results in this region suggests that it rotates around the x-axis on this time scale. This information will be especially useful in evaluating two-dimensional and three-dimensional flow visualizations, because it provides a preliminary range of times over which to look for periodic occurrences in the flow field. If there is a particular aspect of the flow field that emerges with a period on the order of every 20-30 revolutions, then it is likely that it contributes to the oscillation of the side force.

While there are a wealth of data available from the experimental testing that was performed in the 36" VPWT at NSWCCD, there are relatively little data currently available from CFD modeling. At this point, the mean values and standard deviations that were calculated from the computational results correspond very well with the experimental data. The spectral analysis is a little less reliable, because there are simply not enough propeller revolutions completed to allow trends that occur over the course of many revolutions to be recognized through Fourier analysis. It was determined through the course of analyzing the experimental data that lower sampling rates tended to yield better results. This occurs because lower sampling rates result in more revolutions' worth of data per subset. The best low frequency results were obtained from the test runs that recorded data at 500 Hz. These runs contained approximately one minute of data (approximately 600-700 revolutions, depending on the shaft rate) and provided subsets that contained over 8 seconds of data (95 revolutions at a shaft rate of 700 rpm). The latest FFT analysis of the computational data was performed on data that spanned less than 100 revolutions and contained only two subsets, providing very little results over which to take an average. The lowest frequency that can be recognized through FFT is one that completes one cycle during the subset. Clearly, any low frequency response on the order of every $10^2$ revolutions (approximately every 8-9 seconds at a shaft rate of 700 rpm) would be very difficult, if not impossible to detect in the CFD results. As more computational results become available, the frequency analysis will be more accurate.

# 3 VISUALIZATION

## 3.1 Animations

The mean, standard deviation, and root mean square values for the thrust and side force coefficients, in conjunction with the spectral analysis, show that the LES results approximate very closely the effects of crashback. With the results validated, the next step in this research was primarily concerned with using flow visualization and animation to analyze the flow field that occurs during crashback in hopes of determining the physical cause of the unsteady loads. Fortunately, this does not depend as significantly on the availability of additional CFD results as the validation procedure. While it is difficult to visualize flow trends that occur over many revolutions, animations and illustrations can be created to evaluate flow characteristics that affect the thrust and side force magnitudes on a shorter time scale. This will not reveal low-frequency flow trends, but it will help determine the physical causes of the side force. Until now, the focus has been on evaluating and comparing the force and torque data obtained through experiment and computation, but the remainder of the research revolves around evaluating the structure of fluid flow itself.

Data were taken during the VPWT tests using PIV to obtain the velocity vector field in two planes during the experiments. PIV is performed by refracting a laser beam into a laser sheet using a series of optical elements, including a dichoroic lens and beam splitter. The laser light reflects off of tiny, neutrally buoyant particles as they pass through the laser sheet. Video cameras capture closely spaced (temporally) pairs of images, from which particle velocities can be obtained from image correlations between two consecutive images. This provides a two-dimensional look at the instantaneous flow within the fluid. The first plane for which data were taken in the VPWT was the inflow plane for the propulsor, located downstream of the propeller, which records the velocity vectors in the y-z plane. It is the inflow plane, because the reversed propulsor pushes the fluid in the opposite direction of the axial velocity. The second plane cuts along the axis of the shaft to obtain the velocity vectors in the x-z plane. While the PIV data can only be obtained in a two-dimensional plane, velocity vectors in all three spatial dimensions can be resolved because multiple, offset cameras are used to record the velocity data.

Velocity data were also available for the CFD calculations; however, CFD calculates the velocity field for every point within the control volume, clearly providing a more detailed representation of the flow field. This truly three-dimensional velocity field allowed three-dimensional animations to be created for the LES results using Ensight (Computational Engineering International). These animations allow the entire flow to be viewed at once, rather than merely one plane at a time. It is not possible, at this time, to create three-dimensional animations of experimental data, because data can only be taken in a single plane or even a single point during each experimental run. It would be unreasonable to expect that the number of planes necessary to even approximate a three-dimensional flow field could be completed in an acceptable time frame, and it would be impossible with current technology to take data for all these planes at once, during the same test run. This exemplifies one of the major advantages of computational methods over experimental methods.

There are many theories concerning the causes of the unsteady forces and moments that occur during crashback, and three-dimensional visualization may help in evaluating these theories. One theory claims that the forces may result from the creation and shedding of a vortex ring over time (Višohlíd and Mahesh, 2006). Viewing the ring vortex in three dimensions will enable further analysis on its relationship to the resultant loads. The unsteady forces that occur during crashback are, however, directly related to the pressure acting on the blade surfaces. Until now, nobody has investigated the relationship between the fluctuations in pressure, forces, and velocity fields. It was theorized that the flow over each blade separates at different locations and times, resulting in an asymmetric pressure distribution and, therefore, a resultant force. These two ideas provided excellent motivation for the visualization portion of this research. The CFD results provide a full, three-dimensional pressure and velocity field, so both of these concepts can be evaluated in detail. Now that the CFD results have been satisfactorily validated against experimental results, initial steps can be taken to begin investigation into the causes of the forces and moments that were used in the validation. The majority of this step of the research was dedicated to creating and evaluating these animations, attempting to extract the physics behind the unsteady nature of the crashback flow field.

### *3.1.1 Blade Sections*

It was theorized that the unsteady forces acting on the blades were caused by changes in pressure on the surface of the blades. The pressure on the blades is the only physical means of imparting a force, so it was a logical place to begin the flow analysis. If the blades acted like an aircraft wing, then the flow around the blades would remain attached at low angles of attack but separate at higher angles of attack. The twist in the blades from the root to the tip coupled with the non-uniform axial flow through the propeller plane and the rotation of the blades results in angles of attack that vary significantly along the span of the blade. In addition to the span-wise variation, the unsteady nature of crashback also results in a significant time-varying angle of attack. These two flow characteristics provided an excellent starting point for the flow analysis, inspiring the creation of a set of animations designed to provide a general overview of the flow field.

The first set of animations was created so that it would show many different aspects of the flow field at once, in hopes that it would yield a better idea of what specific aspects should be displayed in more detail. This set of animations showed a cross-section of all five blades at the same radius measured from the shaft axis. For this animation, a built-in Ensight function (TempMean) was used to calculate the temporal mean velocity at each point in the control volume. The mean velocities were subtracted from the instantaneous velocities to obtain the turbulent fluctuating velocity at each point. This allows the unsteady nature of the flow to be evaluated more accurately, as the mean flow often masks fluctuations in the visualizations. The mean flow acts as noise, making it very difficult to recognize variations in flow velocity or direction. Removing the mean flow allows only the variations to be shown, represented as green, yellow, and red regions (in order of increasing fluctuation magnitude). In order to assess the flow over the propeller blade cross sections, constant radius surfaces were created and displayed, colored with the magnitude of the fluctuating velocity, and white vectors were added to display the direction of the velocity deviation at all points on the surface. The five blades were displayed at once using multiple Ensight viewports so they could be analyzed simultaneously. Figure 13 shows an example of these animations. A set of animations were completed for three different radii: 1.75 inches, 3.0 inches, and 5.5 inches from the axis of the shaft, providing a clear look at the flow field near the root, middle, and tip of the blades. The “Time” and “Rev” displayed

indicate the solution time and revolution number, respectively, corresponding to the animation frame.

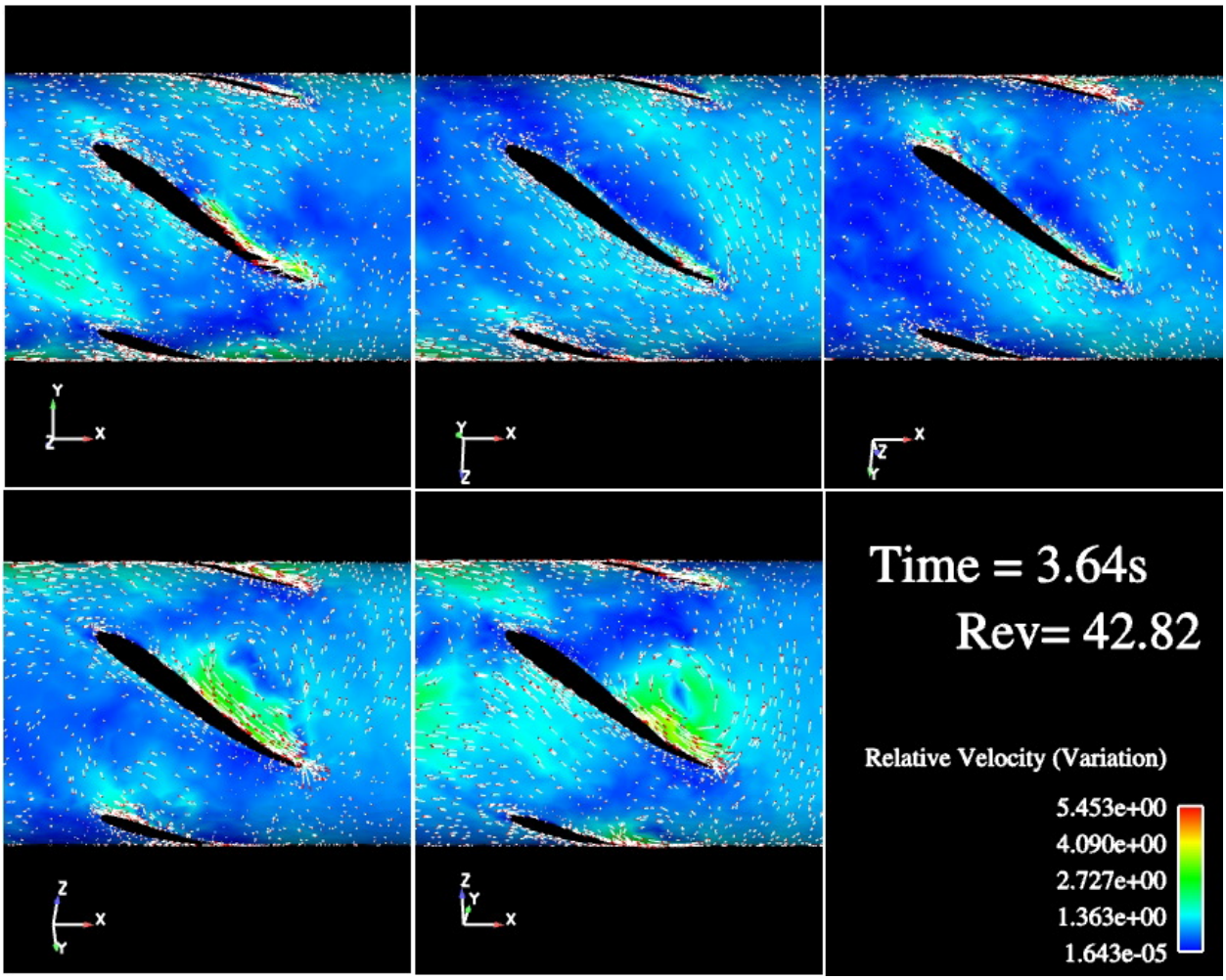


Figure 13- Sample frame from blade section animation (R=1.75 in)

Initially, the five blades were to be evaluated to determine if the location of the flow separation around the blades, represented as areas of large velocity fluctuation, corresponded to the direction of the side force. Upon watching the animations, however, several other flow characteristics became readily apparent. First, the variations in angle of attack near the root of the blade were much greater than those near the tip. The tip angles of attack were much closer to 0° due to the speed at which the tip travels, while the root travels much slower. Fluctuations in axial velocity have a much larger effect on the local angle of attack near the root due to the blade's smaller rotational velocity component. Second, when the animations for all three radii

were viewed simultaneously, it was clear that not only did the separation regions appear on different blades at different times, but they appeared at different span-wise locations as well. The separation regions often appeared first near the root, then, shortly after, farther along the span, and finally near the tip. It seemed as though the separation propagated along the span of the blade. After reaching the tip, the separation region was shed, impacting the blades behind it. The shedding of the separated flow was similar to the tip of an aircraft wing, which leaves a trailing vortex due to pressure differential between the upper and lower surfaces of the wing.

### *3.1.2 Vortex Cores*

The second phenomenon mentioned above prompted the creation of a second set of animations, which was designed to illustrate the formation and shedding of leading edge vortices. Initially, the idea was to use Ensight to create vorticity iso-surfaces in order to visualize the formation and movement of the leading edge vortices. Due to the multiplicity of the turbulence scales, however, the iso-surfaces were so complex that rendering them visually regularly caused Ensight to crash. While visualizing the vorticity iso-surfaces was not possible, Ensight was capable of displaying the cores of the vortices present within the fluid. This set of animations utilized a very powerful tool within Ensight, which determined the location of vortex cores within the flow based on the velocity field provided by the LES code. Initially, the vorticity was also calculated within the control volume using another Ensight function, and the vortex cores were colored using this variable, displaying the strength of the vortex around that part of the core. Unfortunately, there were issues within Ensight that would not allow the vortex cores to be colored in this manner. The second idea was to create a plane perpendicular to the shaft axis, color it using the calculated vorticity, and make it translucent so that both vortex cores located in front of and behind the plane could be seen. There were, again, serious issues with this approach, as Ensight would regularly crash while creating the animations. A new version of Ensight (8.2.3) was installed on the workstation which did not rectify the second problem but did allow the first approach to be utilized. The side force was represented as a white vector corresponding to its magnitude and direction. This was added to help determine if the location of the vortices corresponded with the direction of the side force. Figure 14 shows an example of the animations created displaying the vortex cores within the flow. The downstream side of the

blades is shown on the left, and the upstream side of the blades is shown on the right, which means that the blade is rotating counter-clockwise in the left half of the frame and clockwise in the right half of the frame.

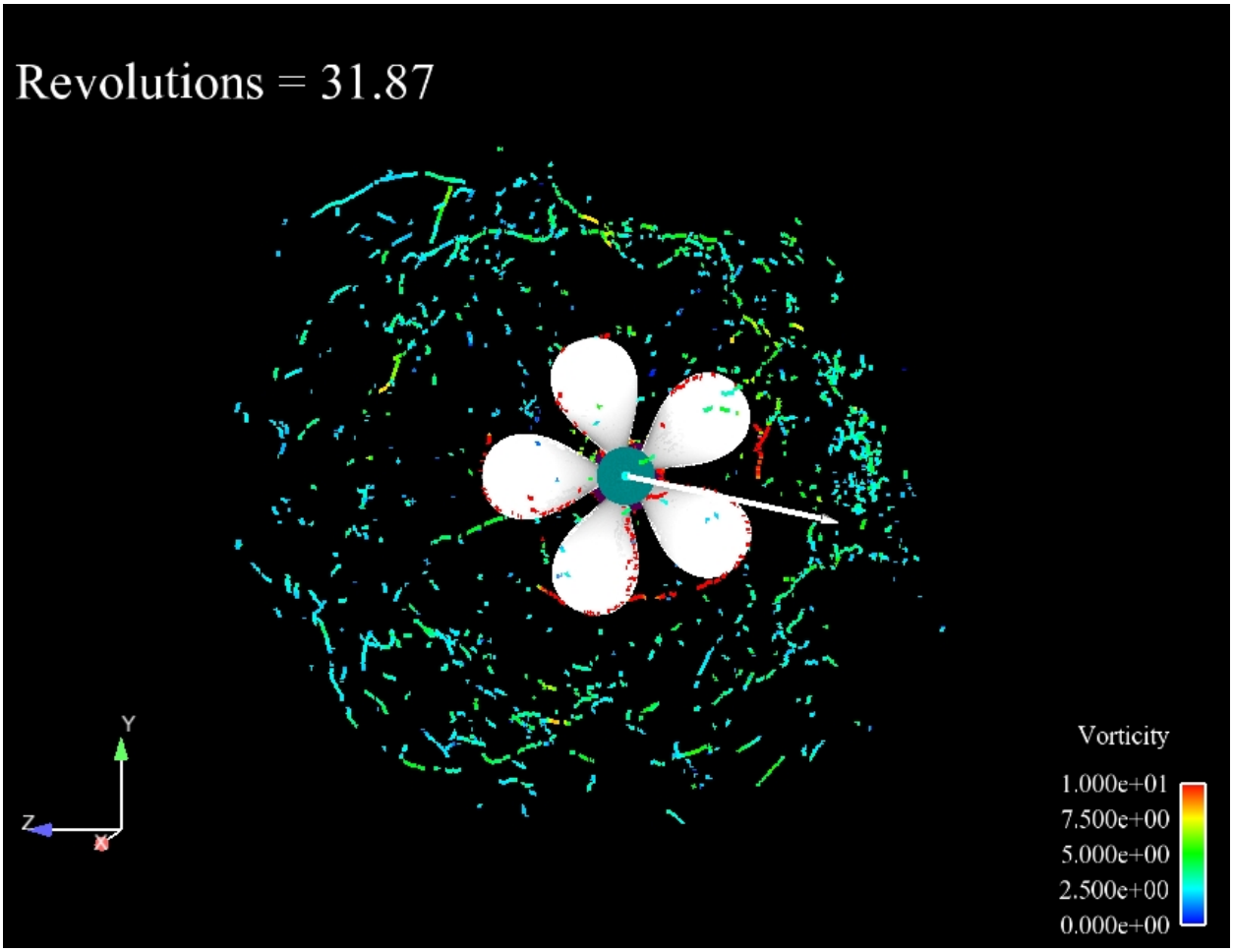


Figure 14- Sample frame from original vortex core animation.

While it was not the original purpose of the animation, the cores which lie just outside the propeller tips clearly support the existence of a ring vortex as was expected. These cores generally lie in the tangential direction, forming a circular shape just outside the blade tips, which indicate that the ring vortex is a torus shape that is located near the tips of the propeller blades. While this is encouraging, the most interesting discovery was made closer to the blade root. Figure 14 also shows the existence of vortex cores that are located along the leading edge of several of the blades, colored red due to the strength of the vortices. In analyzing the

animations, this vortex clearly originates near the blade root and propagates along the leading edge of the blade, supporting the theory developed in analyzing the blade section animations.

While this animation illustrated several new physical structures within the crashback flow field, several problems arose. First, it was impossible to determine the axial location of the vortex cores that existed in the ring vortex. Second, it was nearly impossible to compare the angle of the side force converted from the LES results for use in validation, because the angle was measured in the inertial reference frame, while the animations represented the system in the rotational reference frame. In other words, the side force results from the simulation had been converted to the inertial reference frame for comparison with the experimental data, but the animation (including the side force) was still being shown in the rotational reference frame. In order to correct these issues, the same animations were recreated, adding a side view of the propeller which gave a better idea of the location of the axial location of the vortex cores. A function was written in Ensight that rotated the propeller and flow field each frame by the angle corresponding to the amount the propeller would have actually rotated in the amount of time that passed between frames, resulting in the animations being shown in the inertial reference frame. This not only allowed the side force angle to be more accurately determined, but it also slowed down the relative rotation of the vortex cores, making the animation easier to analyze. Figure 15 displays a sample frame of the new animation.

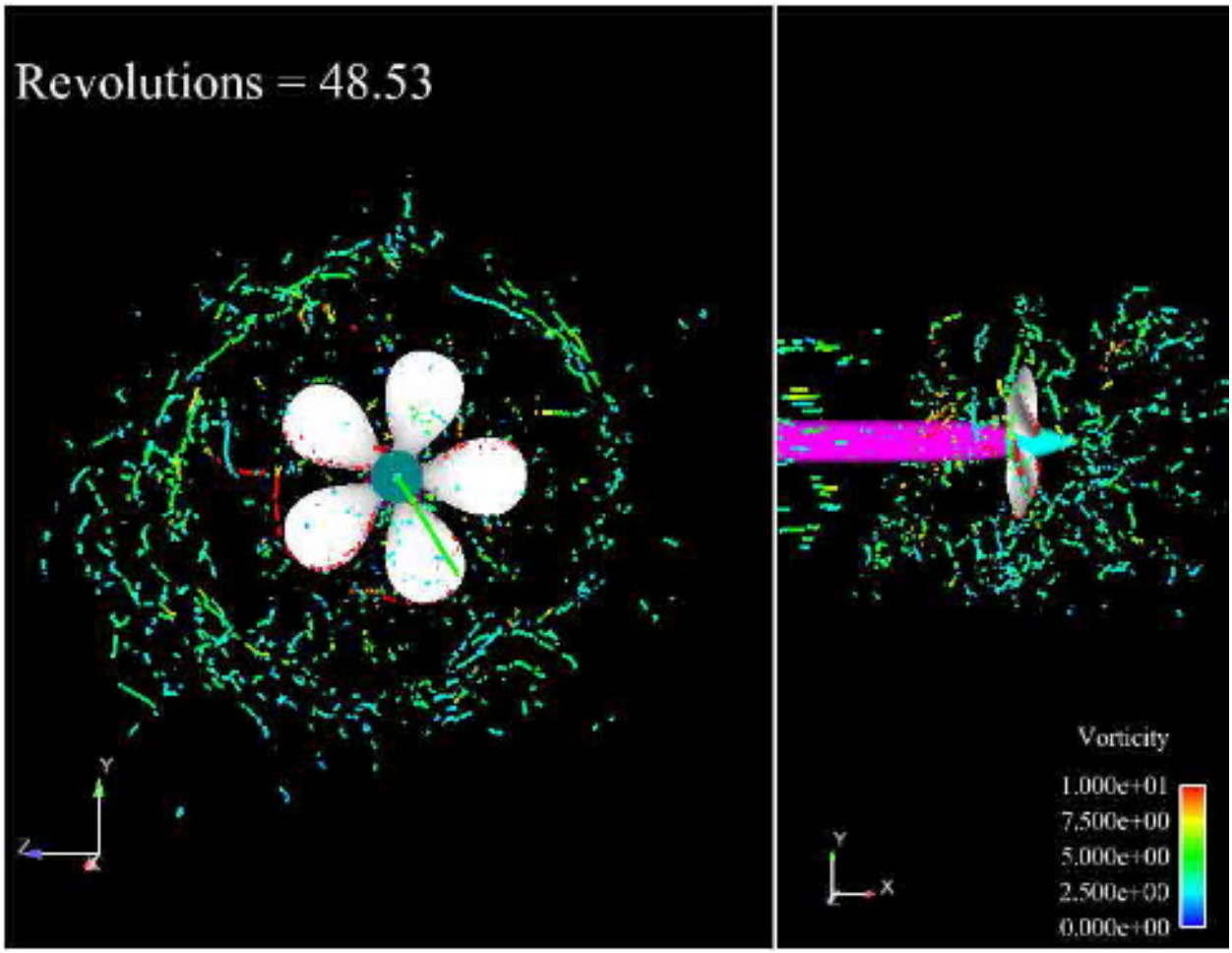


Figure 15- Sample frame from new vortex core animation.

### *3.1.3 Pressure*

The third set of animations created displayed two axial views of the propeller blades, one from downstream (left side of Figure 16) of the propeller and the other from upstream (right side of Figure 16). The propeller blades were colored by the pressure distribution over them, and white vortex cores and a red side force vector were displayed. One of the main purposes of this animation was to determine the relationship between the pressures on the blades and the formation of the leading edge vortices previously mentioned. The second purpose was to understand the relationship between the pressure on the blades and the side force. Finally, the two relationships were compared to determine any correlation between the vortices and the side force. The same problems arose for this set of animations as the previous set, with regard to the

reference frame, and similar measures were taken. It was determined that the axial location of the vortices was less important for this animation, as the vortex cores of concern were located on the blades rather than the space around the blades. It was important, however, to ensure that the animations were in the inertial reference frame, so the propeller was rotated similar to the previous set of animations.

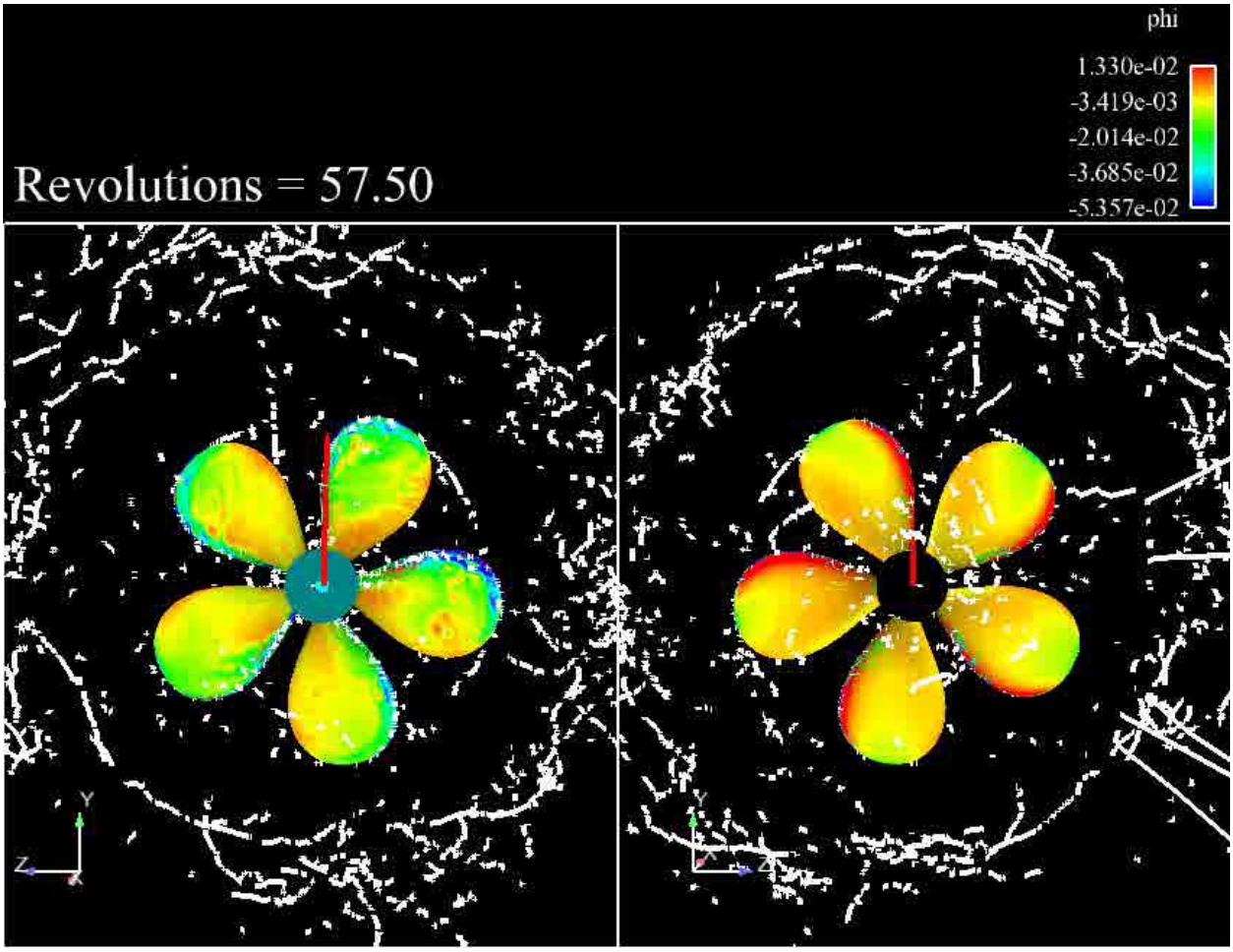


Figure 16- Sample frame from pressure animation.

## 3.2 Analysis

Even fairly cursory evaluations of these animations have yielded a wealth of information about the crashback flow field. While initial analysis did not provide the insight necessary to properly understand crashback, it did provide enough information to create other animations which display more specific and relevant aspects of the flow field. In order to truly understand

the crashback phenomenon, these animations were analyzed in detail. This analysis was comprised of two major parts: first, the animations were observed at several different playback speeds to get an overall feel for how the flow field acts during crashback, and second, specific frames were selected and then compared and contrasted with frames with either comparable or highly dissimilar measurable quantities, such as thrust and side force magnitude and direction. These two methods each provide different benefits to the analysis, with the animations providing an overview of the unsteady nature of the flow field and the still frames providing detailed information about the flow at specific times.

Viewing the animations as videos rather than as still frames provided the advantage of getting an excellent feel for the unsteady nature of the flow field. Depending on the animation, specific flow field characteristics could be viewed to determine their formation, movement, and dissipation. One of the most useful aspects of the animations was the ability to watch the relative movements of flow features, propeller blades, and resultant forces.

While the animations offered an overall appreciation of the flow field, still frames gave a more exact impression of what is going on at a particular point in time. This was useful in determining how the location of a vortex or the pressure distribution affected the direction and magnitude of the side force. For this research, two approaches were used to evaluate still frames taken from the animations. First, frames were taken from points in time that had similar side force magnitudes or angles. Second, frames containing very dissimilar side force magnitudes and angles were contrasted. Using still frames also allowed aspects of the flow field at different times that have similar (or extremely different) characteristics to be compared and contrasted to determine which aspects of the flow had the greatest influence on the flow field and resultant loads.

### *3.2.1 Blade Sections*

The first animation created was designed to provide a wealth of information about the flow field around the blades in order to determine what would be the eventual focus of the analysis. The blade section animations proved very useful in this respect, displaying certain aspects of the flow field that had never previously been seen. The analysis was initially

performed with this purpose in mind; however, these animations proved useful in more than just this capacity.

In order to gain an appreciation for the entire flow field at once, the animations for all three radii were synchronized and viewed simultaneously. Within a few viewings, two particular aspects of the flow field became clear. First, vortices formed on the leading edge of the blades near the root and propagated along the length of the leading edge, eventually shedding from the blade tips. The sequence of images shown in Figure 17 displays the movement of the leading edge vortices along one of the blades.

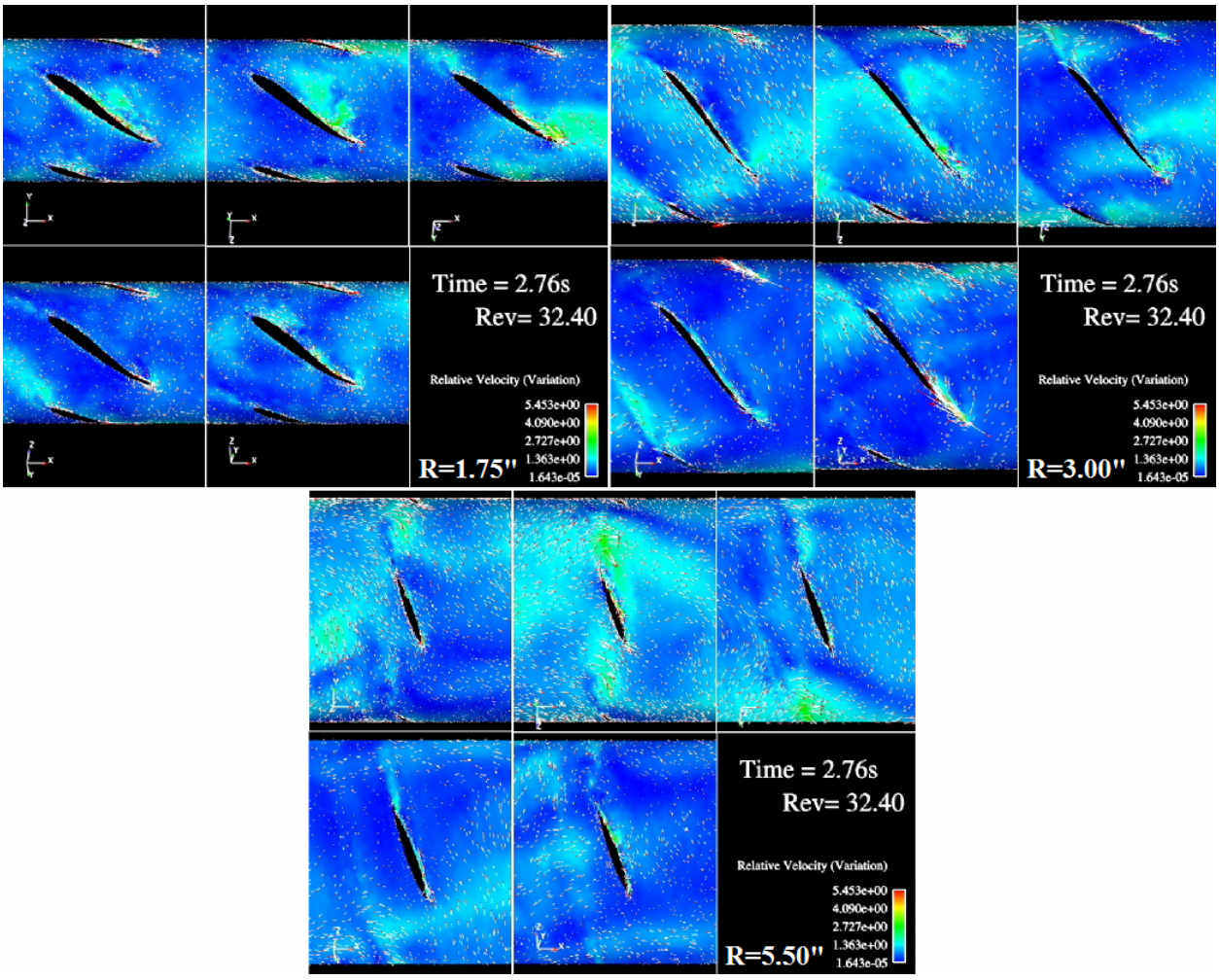


Figure 17- This blade sections animation frame shows a vortex at the leading edge of the third blade (top right of each set) near the root (top left set).

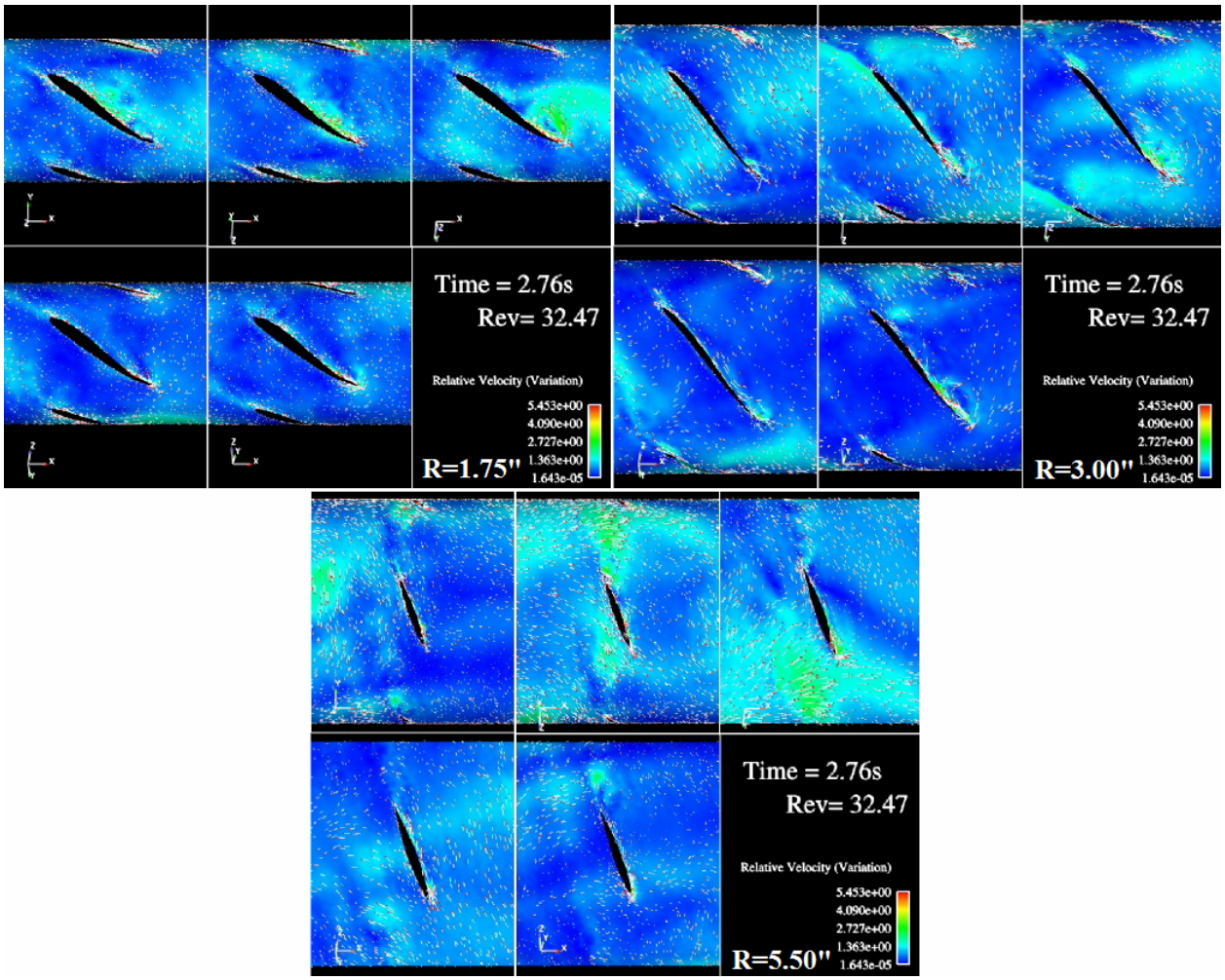


Figure 18- This blade sections animation frame displays a leading edge vortex on blade three near the middle of the blade (top right set).

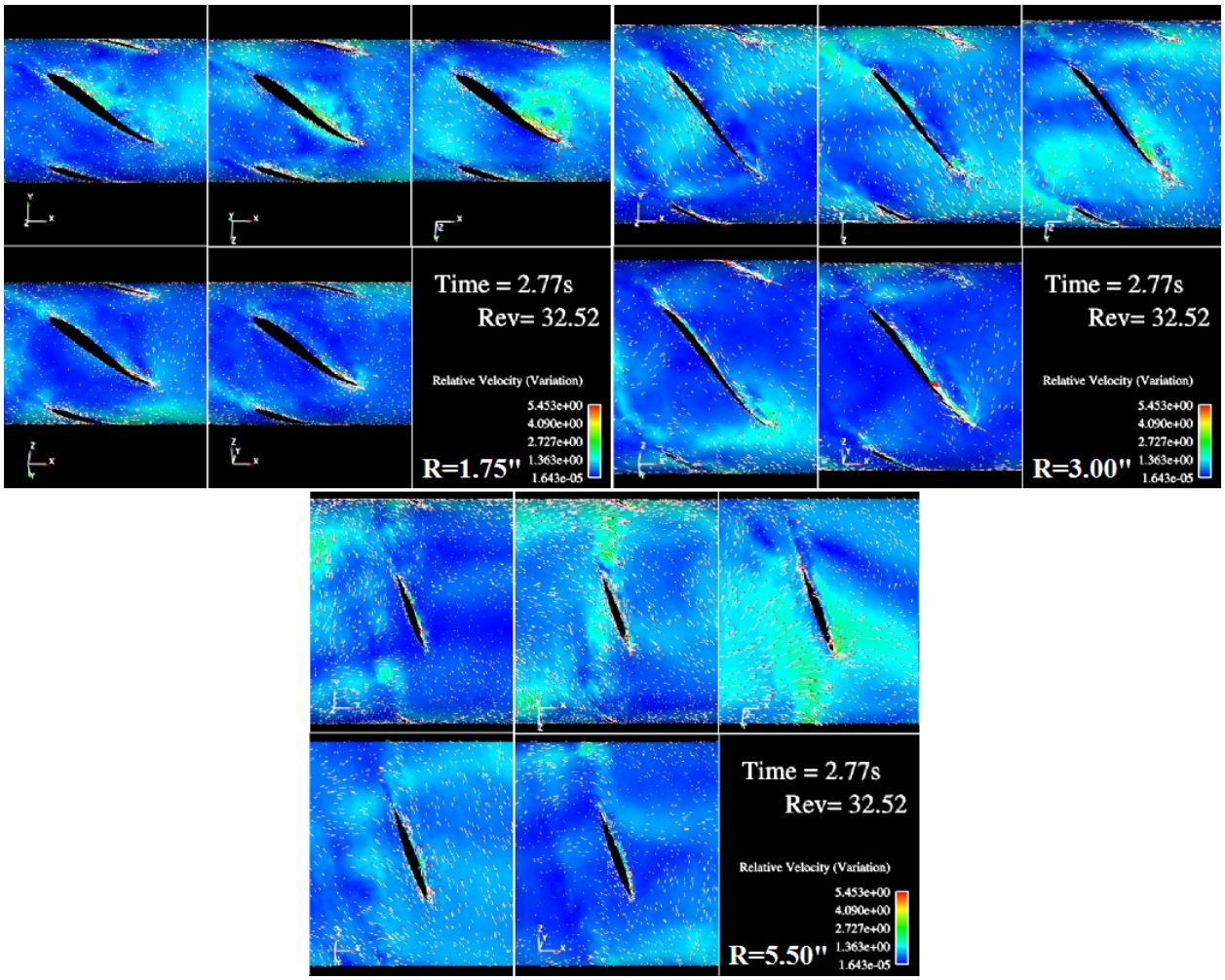


Figure 19- This blade sections animation frame shows a leading edge vortex near the tip of blade three (bottom set).

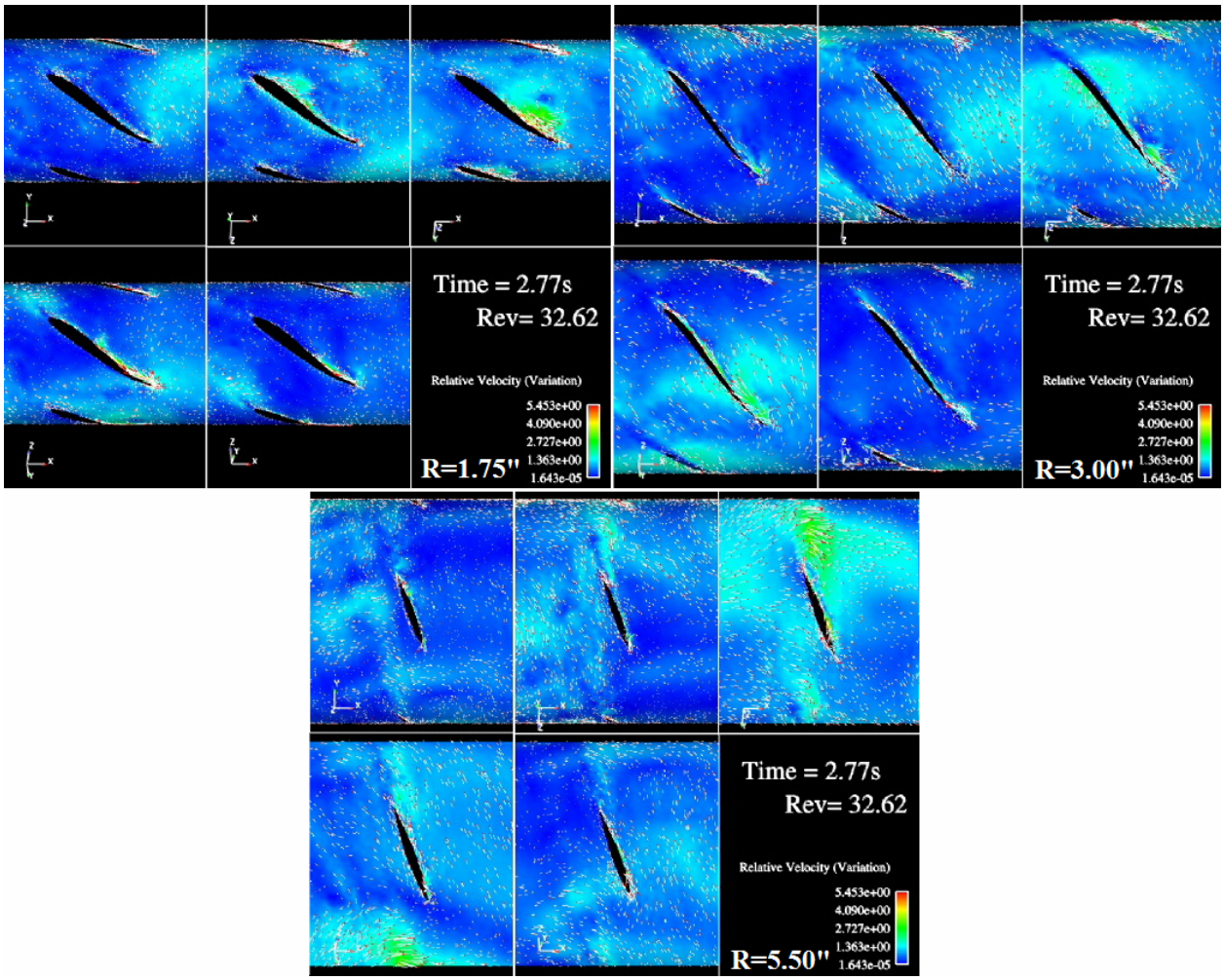


Figure 20- This blade sections animation frame shows the vortex being shed off the tip of blade three.

In these animations, the color and vectors displayed represent the deviations of the flow from the mean. Because the velocity fluctuations are displayed, vortices were theorized to be represented by the areas that are not colored blue (areas of large velocity fluctuations). This theory is supported by the presence of leading edge vortices observed in subsequent animations. In Figure 17, the vortex can be seen near the root, then a few frames later (Figure 18) at the middle radius on the same blade, then near the tip of the blade (Figure 19). Finally, Figure 20 shows the leading edge vortex being shed off the tip of the blade. It is theorized that these vortices are a result of drastic changes in the blade's angle of attack near the root. Similar to an

aircraft wing, the angle of the flow as it reaches the blade determines how the fluid will move over the “airfoil” in that region. The combination of the blades’ twist and angular velocity results in the root having a much higher mean angle of attack than the tip. The high angle of attack means that even slight changes in the fluid flow could result in flow separation, causing the formation of vortices near the root. These vortices travel up the leading edge of the blade and are shed off the tip of the blade. It was theorized that these vortices could affect the pressure on the blade surfaces enough to affect the magnitude of the side force, prompting the development of other animations, which displayed combinations of vortex core locations, vortex strength, and pressure distribution.

The second characteristic noticed was that vortices ingested by the propeller were impacting each blade in sequence as it rotated through the vortical region. Not all of the vortices in the animations propagated along the leading edge of the blades; other vortices seem to only affect the blades near the root. These vortices are either be ingested directly into the propeller blades, carried into the propeller plane by the fluid flowing into it, or are formed at the blade roots and dissipate before reaching the tips. Regardless of their origin, these vortices affect the flow over each blade with a high level of periodicity. As the blades rotate around the propeller, they pass through the vortex repeatedly until its axial location moves upstream of the propeller blades. This is represented in the sequence of illustrations shown in Figure 21.

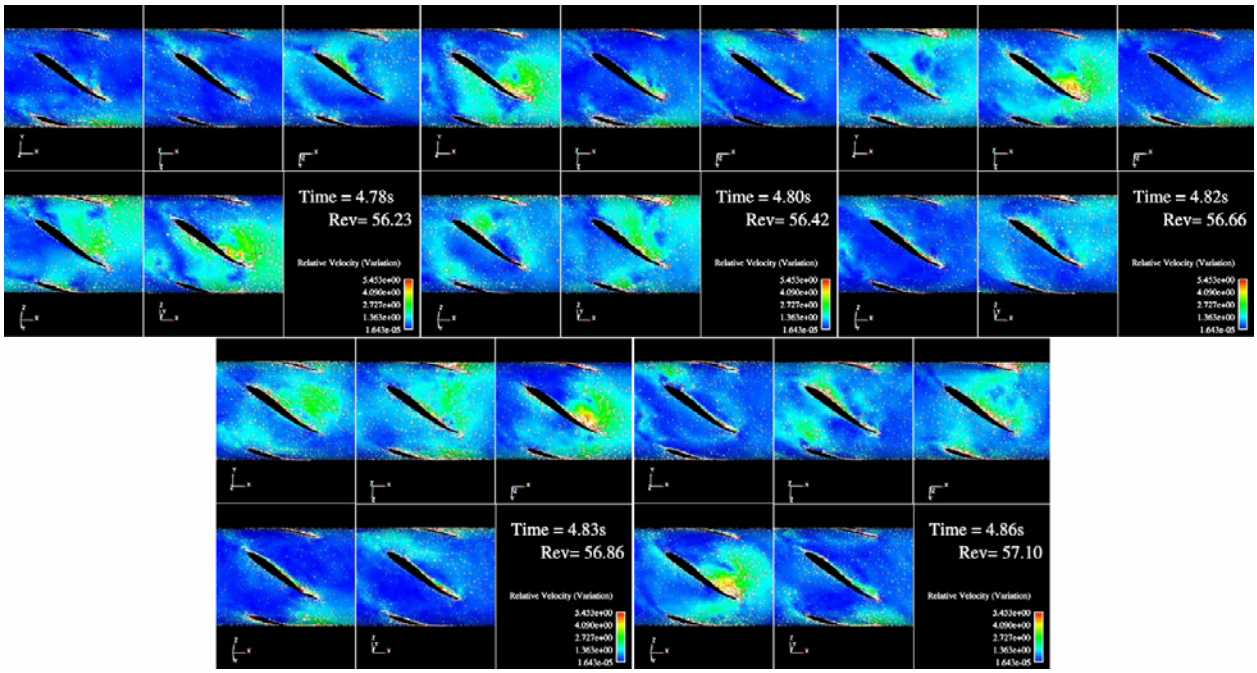


Figure 21- Blade sections animation frames showing the impact of a vortex on successive blades (R=1.75")

In Figure 21, the vortex impacts the fifth blade (bottom center blade) in the first frame. The second frame shows the vortex impacting the first blade (top left blade), followed a few time steps later by impacting the second blade (top center blade) in the third frame. The fourth frame shows the vortex on the third blade (top right blade), and finally, the fifth frame shows the vortex impacting the fourth blade (bottom left blade). Clearly, the rotation of the propeller results in vortices affecting each blade in sequence as it passes through the propeller plane. As previously mentioned, this was noticed very early, but its significance did not become apparent until after the completion of a specific set of illustrations that were inspired by further pressure distribution evaluation. This will be referenced and discussed in detail with that portion of the analysis.

### *3.2.2 Vortex Cores*

This animation was inspired by the leading edge vortices that were discovered in the blade section animations. It was theorized that the side force direction and magnitude might be related to these leading edge vortices. The initial animation (shown in Figure 14) showed only an axial view of the propeller, but it became instantly clear that, in addition to the leading edge

vortices that the animation was intended to show, the animation displayed the ring vortex near the blade tips. The second vortex core animation was created, because the visibility of the ring vortex provided for the evaluation of Višohlíd and Mahesh's claim (2006) that suggested the vortex ring shape, orientation, and axial location might also affect the forces acting on the propeller. The second animation literally added another dimension to the vortex core analysis.

Upon viewing the animations, no clear relationship between the leading edge vortices and the side force became apparent. At first, it seemed like the side force direction corresponded with the location of the leading edge vortices, but contradictions were continually observed throughout the animation. Often times, the side force would be directed just ahead of the first blade (of several consecutive blades) with a prominent leading edge vortex, as shown in Figure 22. Other times, there would be a series of blades with leading edge vortices but no side force, exemplified by Figure 23. While initially the side force direction seemed to be dictated by the existence and location of leading edge vortices, it seems more likely that both the vortices and side force were both a result of another flow characteristic.

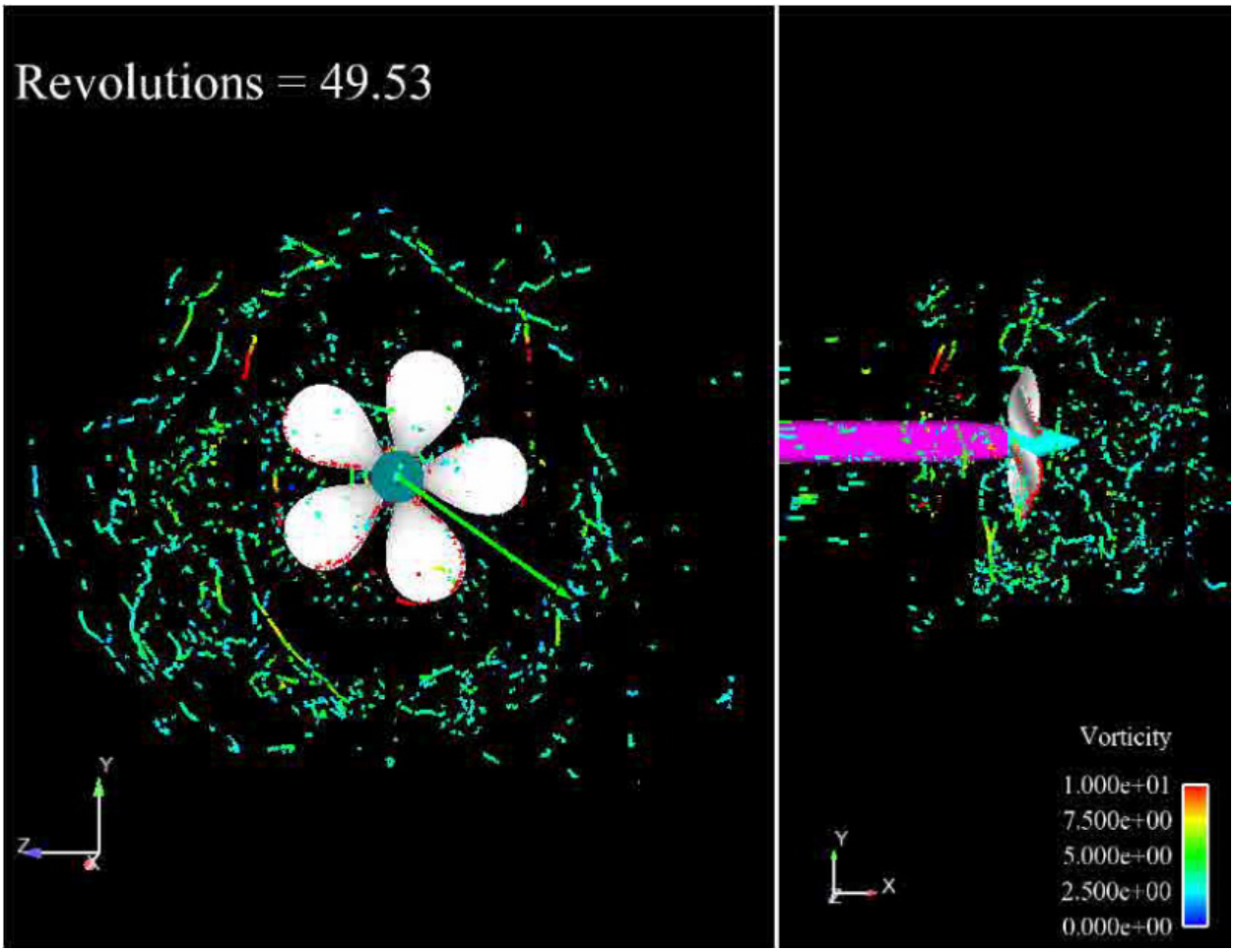


Figure 22- Vortex core animation frame displaying the side force direction correlating with leading edge vortices.

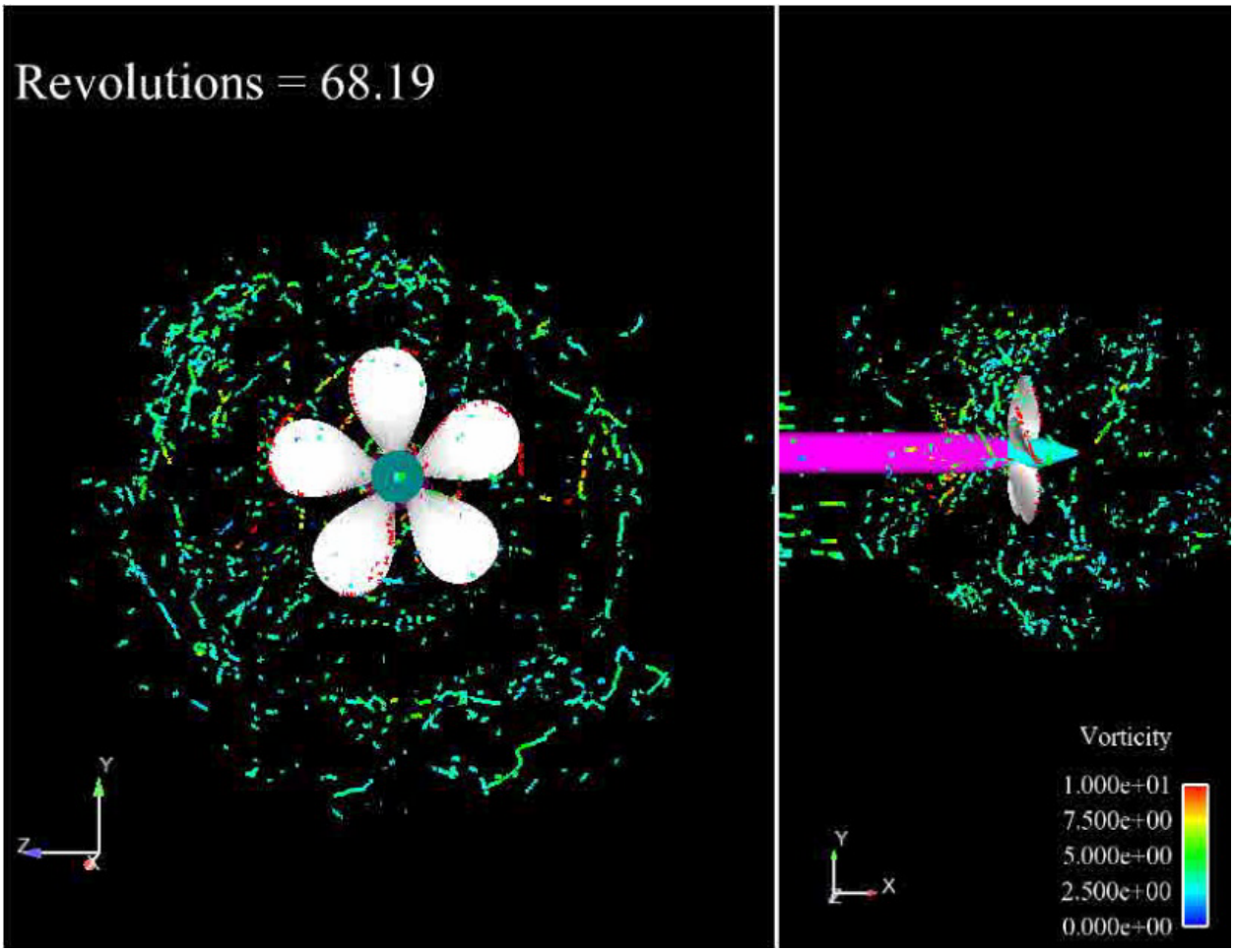


Figure 23- Vortex core animation frame showing leading edge vortices with a very small corresponding side force.

Both Figure 22 and Figure 23 show similar leading edge vortices, but the corresponding side forces differ significantly. At first, it was theorized that the large side force could possibly be caused by only asymmetrical vortex formation, suggesting that the forces due to symmetrical vortices would cancel each other out. Clearly, however, both figures above display blades with and without leading edge vortices, indicating that this theory is invalid.

The vortex core animations were also used to determine whether the effect of the vortex ring shape and orientation had any effect on the side force. The vortex core animation clearly supports the existence of the ring vortex. It is represented by the circular region of vortex cores just outside the propeller blades. These cores are predominantly in the tangential direction, indicating that the vortex is shaped like a torus and is located just outside the propeller disc. The

animations show that the vortex ring rotates about the propeller axis at a speed significantly lower than the propeller itself. This research was unable to determine the period of this rotation, because there was no capability available to track individual vortices. The density of the vortex ring also changes with time. Some portions of the animations appear to have many more vortex cores present than others. In addition to the density changing with time, it also changes with radial location; in fact, the ring vortex is only very rarely symmetrical. This can be seen in Figure 22 and Figure 23. Note the low vortical density in the upper right portion of Figure 22 compared to the high density area in the lower left. Also, note the relative angular location of the high and low density areas compared to Figure 23.

Still frames were taken from this animation to determine whether the vortex ring had any impact on the side force. First, frames were taken from times when the side force was particularly large, as can be seen in Figure 24 and Figure 25. The analysis of these still frames revealed no evidence that the orientation of the ring vortex had any effect on the direction of the side force. Some frames showed the side force pointing directly at a very high-density portion of the ring vortex (Figure 24), while others illustrate the side force pointing toward a relatively low-density area of the ring vortex (Figure 25). Even though both the side force and vortex ring rotate around the shaft axis, it is clear that they have little, if any, relationship. Analysis of the vortex ring rotation period/frequency could prove helpful in this regard.

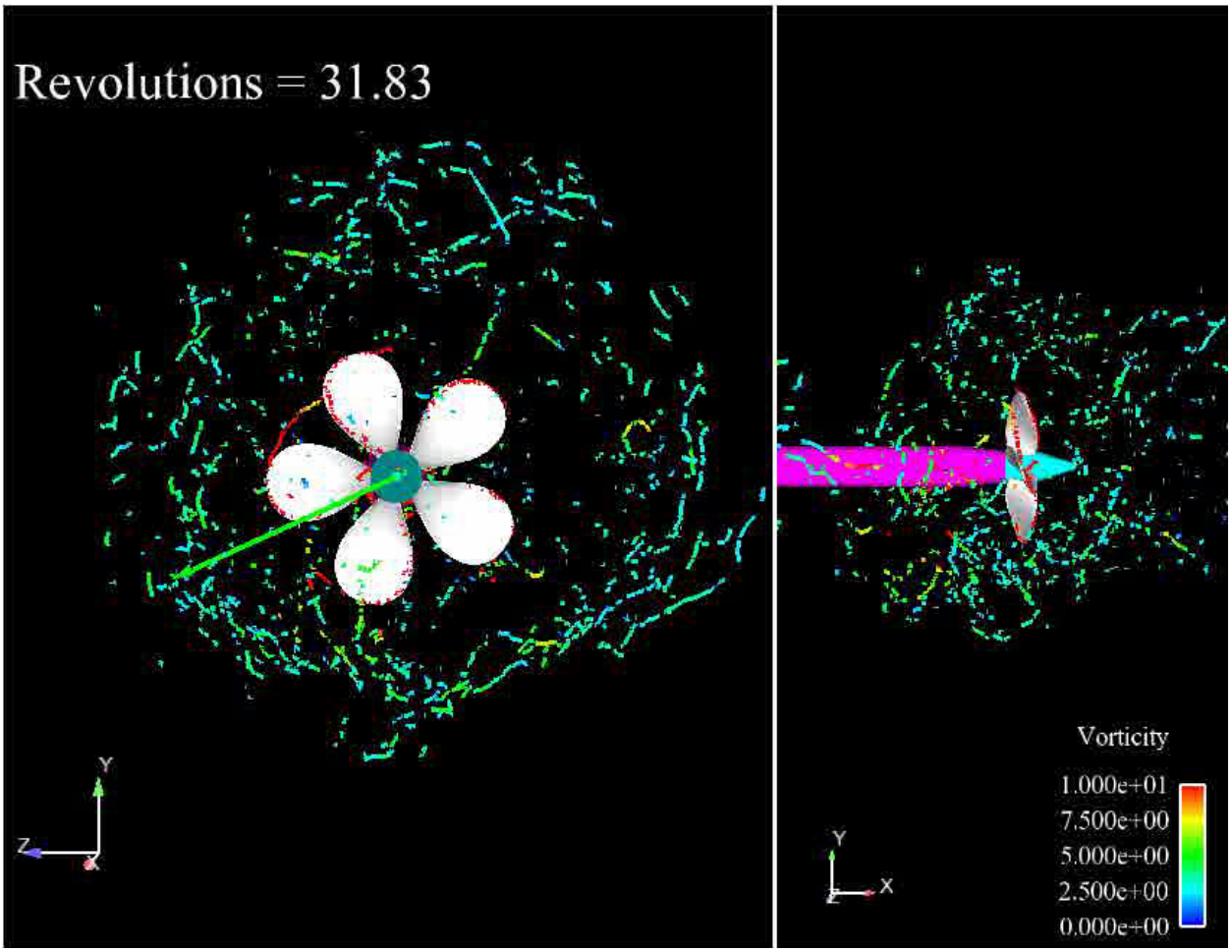


Figure 24- Vortex core animation frame displaying a large side force directed toward high-density portion of ring vortex.

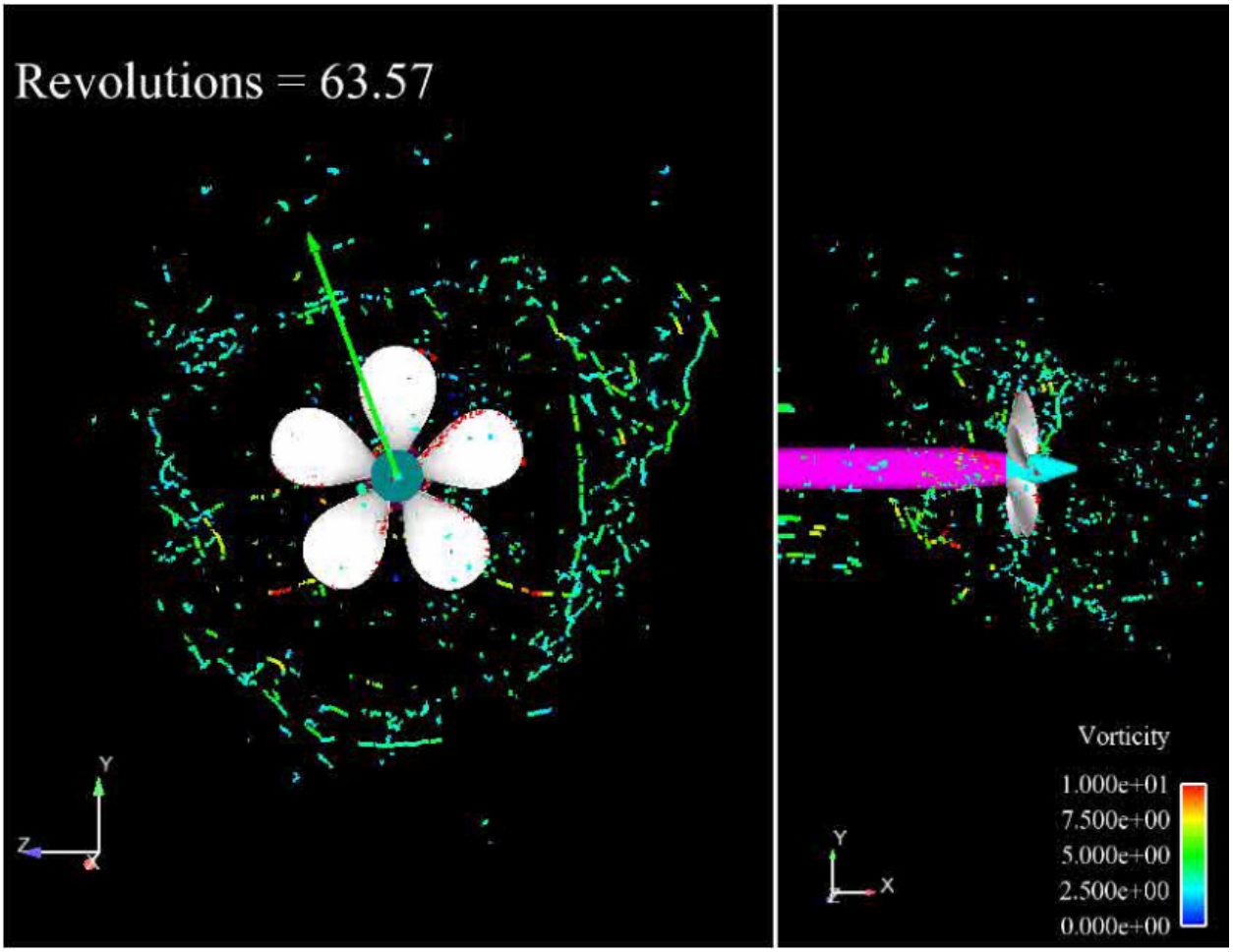


Figure 25- Vortex core animation frame showing a large side force vector directed toward a very low-density area of the ring vortex.

In addition to analyzing the effect of the vortex shape, density, and orientation on the side force, the axial location of the ring vortex was observed in hopes of finding a correlation with the thrust. As can be seen in the vortex core animation frames shown thus far, it is extremely difficult to quantify the axial location of the vortex ring. The ring is not established enough to visually determine the axial location, so no correlation was determined.

### *3.2.3 Pressure*

This set of animations was also inspired by the blade sections animation. The vortices noticed in the blade sections animation would result in a pressure change on the blade surface, so this animation was created to display the pressure distribution on the blades and determine its

effect on the side force. Figure 26 shows the pressure distribution over the blades for a frame that corresponds to a large side force. As previously mentioned, the downstream side of the blades is shown on the left (blades rotate counter-clockwise), and the upstream side of the blades is shown on the right (blades rotate clockwise).

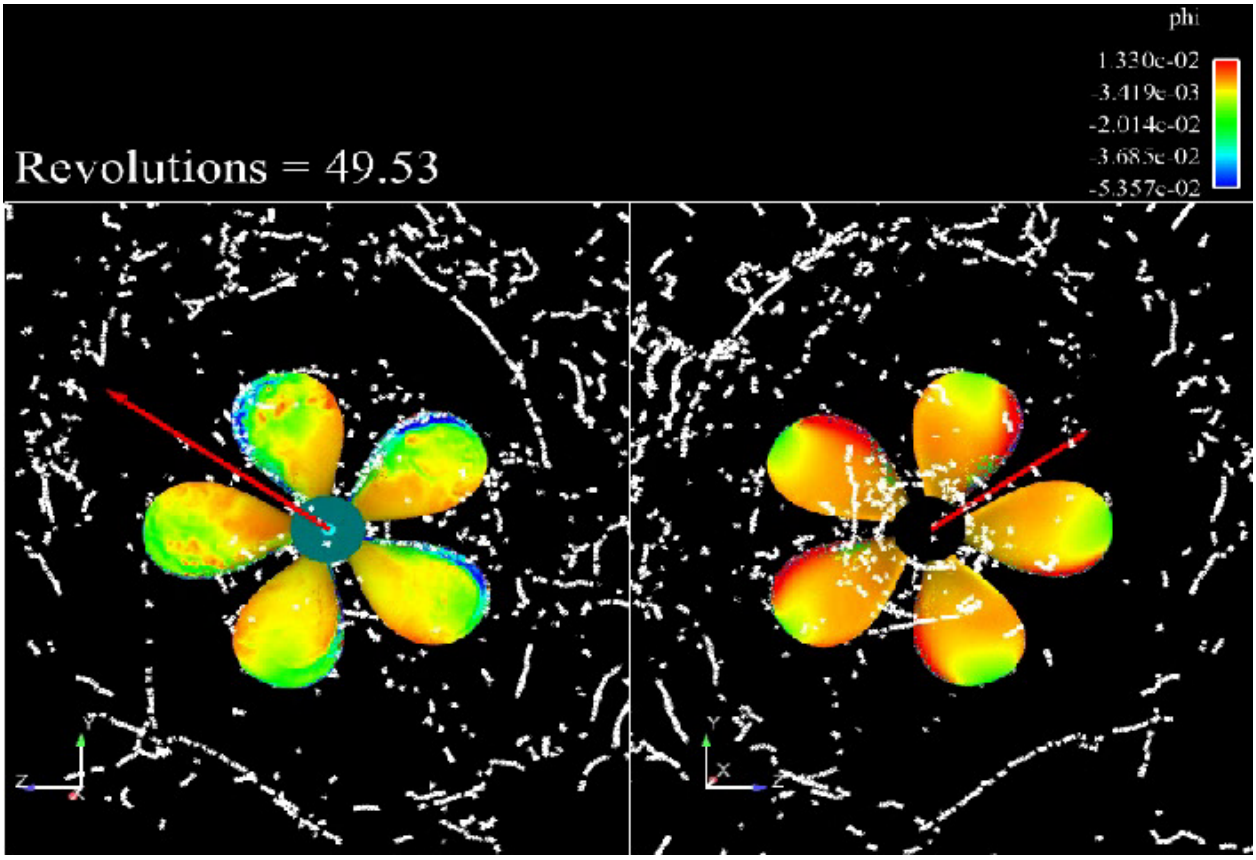


Figure 26- Pressure Core frame corresponding to a large side force.

In order to determine which area of the blades on which the analysis should focus, the profile area of the propeller from the direction of the side force was examined. It was theorized that the blades that extend nearly perpendicular to the direction of the side force would have the most influence on its magnitude, because their area has a normal vector that is predominantly in the side force direction and would have the greatest area over which the pressure could affect the side force. The twist on the blades results in the area of these blades near the root having the most significant impact on the side force. Clearly, the twist on the blades results in a portion of the resultant pressure force lying in the axial direction, but this is absorbed into the thrust,

leaving just the side force to act perpendicularly to the shaft axis. The focus of the analysis was to determine if the pressure had any affect on the side force, so this assumption focused the analysis on the root region of the blades most perpendicular to the side force.

Initial analysis showed little correlation between the side force and the pressure distribution. Actually, the pressure distribution seemed to indicate that the side force should act in the opposite direction than it actually did. In Figure 26, the blades located at 2 o'clock and 4 o'clock in the left half of the illustration have a low pressure region on the leading (counter-clockwise facing) edge. The corresponding blades in the right half have a high pressure area near the leading edge. The twist on the blade is such that the low pressure surfaces face away from the side force, and the high pressure sides face toward it, suggesting that the resultant force on that blade is actually in the opposite direction of the side force. The other blades that are nearly perpendicular to the side force do not have nearly the pressure differential that the first blade does, so it is unlikely that the pressure differential on those blades will affect the side force enough to overcome the force suggested by the pressure distribution on the first blade. All of the blades have a relatively high pressure area near the trailing edge and root in the left half of the illustration, and all the blades have a fairly symmetric high pressure distribution on the surfaces in the right half if the figure. This symmetry suggests that the resultant force would be relatively small, contradicting the large side force displayed.

The pressure distribution animations shown in Figure 26 made it very difficult to determine which blades (or portions of the blades) had the greatest effect on the resultant side force. In order to determine this, the Force function in Ensight was going to be used to calculate the "force distribution" on the blade surfaces based on the pressure distribution. Because the force would have been a vector, it would have been possible to calculate the force that was being applied in the direction of the side force. This would have been used to color the blades, thus displaying which areas had the greatest effect on the side force. Unfortunately, the Force function did not work due to a bug in the multi-processor version of the Ensight code. This bug has subsequently been fixed but after this research had been concluded.

One of the main reasons this animation was not as useful as it was designed to be was that the pressure caused by the rotation of the propeller made it difficult to recognize the fluctuations in pressure due to vortices and other flow characteristics. The instantaneous

pressure is driven primarily by the rotation of the blades rather than the unsteady flow. The mean pressure due to this rotation is practically symmetrical, resulting in a side force that is nearly zero. Because the magnitude of the mean pressure is so large compared to the fluctuations, it is very difficult to determine their effect on the side force. Similar to the way the mean velocity field hid the fluctuations by acting as noise, the mean pressure distribution masked the variations in pressure. In order to rectify this, several frames and short animations were created that displayed the turbulent pressure fluctuations rather than the pressure distribution in order to determine if these fluctuations had any effect on the side force direction or magnitude. Figure 27 shows an example of the frames that were created. Frames that had particularly high or low side force magnitudes and frames that had similar side force angles were used in this portion of the analysis. There was not enough time to generate full animations for the same number of revolutions as the other animations; however, short animations were created and frames were taken for many different times and conditions throughout the simulation, providing a fairly representative sample of the results.

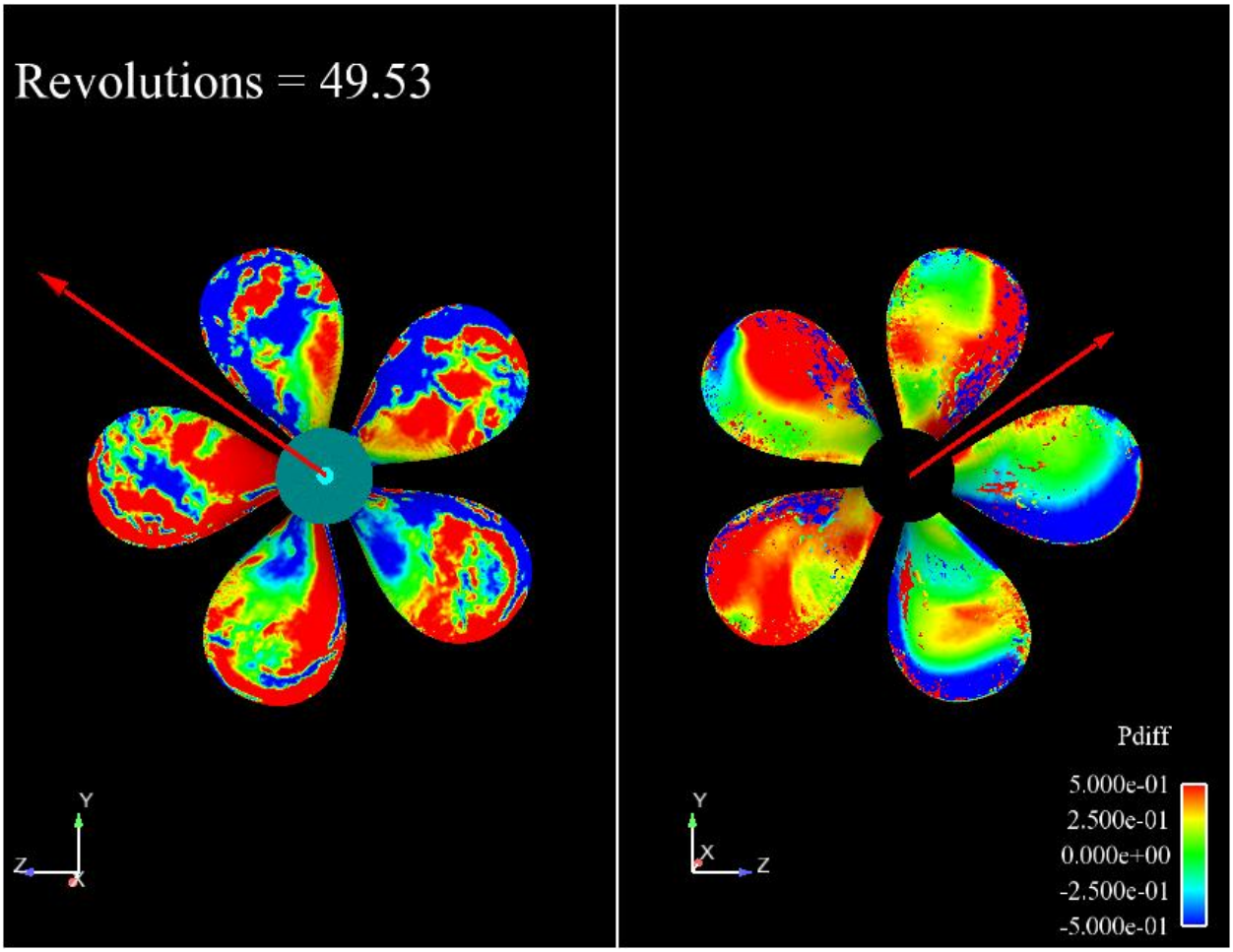


Figure 27- Pressure fluctuation illustration with corresponding side force vector.

In Figure 27, the blade at 2 o'clock in the left half of the illustration has significantly higher pressure than the mean in the central portion of the blade near the root, and it is twisted such that this portion of the blade has the greatest profile area and twisted such that if faces in the opposite direction of the side force. The other side of the same blade (10 o'clock in the right half) has a pressure distribution close to the mean, and the blade is oriented such that this side faces the same direction as the side force. This pressure differential would result in a force that acts in the direction of the side force. The blade on the opposite side of the propeller, at 7 o'clock, in the left half (5 o'clock in the right) has a pressure close to the mean on the side of the blade facing away from the side force and a lower pressure on the side facing the side force, which would result in a force in the same direction as the side force. This correlation suggests

that fluctuating pressure, rather than the instantaneous pressure, has a greater effect on the side force. Figure 26 and Figure 27 illustrate the instantaneous and fluctuating pressures at the same time. Clearly, the expected resultant force, based on the pressure distribution over the blades with the greatest profile area, is significantly different. The instantaneous pressure distribution is so symmetrical that it is difficult to determine a side force direction, whereas the pressure fluctuations indicate that the force would correlate better with the displayed side force.

The analysis of the pressure variations that led to this conclusion directed the analysis back to an observation from the blade sections animations. It was observed and noted earlier that the blades would pass in sequence through vortices that were generated near the blade root or ingested into the propeller plane. While initial analysis of the leading edge vortices revealed no correlation with the side force, if these vortices cause a significant increase or drop in pressure on multiple blades, then they could have a significant impact on the side force. This would also explain a phenomenon noticed during the spectral analysis portion of the LES validation.

The spectral analysis showed a significant response for all the results at the blade rate which was largely ignored to this point, because the focus had been on determining the cause of the low frequency results. With the new evidence that the side force correlates with the pressure variation on the blades, a new theory was developed. If the vortices being ingested into the propeller plane are impacted by the blades at a frequency equal to the blade rate, the resulting force will also fluctuate at the same frequency. The majority of these vortices are not significant enough to create a large side force, but there is still a small resultant side force that oscillates at this frequency. The large side forces are created in much the same manner as rogue waves at sea. In a storm where there are 20-30 foot rolling seas, the individual waves are manageable and may not result in much damage. If several of these waves collide, however, their magnitudes sum, and a gigantic rogue wave is created that is capable of destroying vessels unlucky enough to be in the vicinity. The new theory treats the effect of these vortices on the blade pressure as rogue waves. Small vortices, or even a larger vortex, acting on a single blade may not have a great enough effect to result in a large side force. A vortex or series of vortices that act on several blades simultaneously, however, could result in a large resultant force.

When watching a short pressure fluctuation animation, it became clear that the side force increases when the pressures on the blades perpendicular to the side force fluctuate away from

the mean and decrease when the magnitude of the variation decreases. As the blades pass through a vortical region, the pressure increases on the side of the blade facing away from the side force and a pressure decrease on the side of the blade facing toward the side force. These disturbances vary directly with the side force magnitude. A fraction of a second later, the blades leave the vortical region, the pressure variations decrease, and the side force drops. Immediately after, two more blades are affected by the vortices as they rotate through the same region, and the pressure variation increases again, resulting in an increase in side force magnitude. This process continues until the axial location of vortical region changes enough that the propeller blades no longer pass through it. While a propeller operating in a steady state, such as simple forward operation, would have fairly consistent pressure distributions over its blades and show few fluctuations, the crashback animation shows highly dynamic pressure variations. The pressure on the blades changes drastically from when it approaches perpendicular to the side force on one side to when it approaches parallel with the side force to when it becomes perpendicular on the other side of the side force. Clearly, the larger and more intense these regions are, the more impact they have on the pressure distribution and the greater side force they create.

This not only affects the magnitude of the high frequency oscillations, but it also affects the magnitude of the low frequency oscillations. The low frequency effects are due to the overall rise and fall of the side force, thrust, and torque as the vortices move through the propeller plane. For example, if there were no large vortices passing through the plane, the oscillations would be very small, but with the introduction of large vortices, the peak side force increases as the vortices affect the propeller blades more and decreases as they exit the propeller plane. This process is much slower than that of the blades impacting the vortices, so the frequency at which it occurs is much lower. In order to quantify this process, the vortices must be somehow tracked and their movement recorded. As of now, there has been no analysis performed in the tracking of specific vortices. The axial component of the velocity through the propeller disk was estimated by creating a plane perpendicular to the shaft axis in the center of the propeller in Ensight and coloring it with the axial velocity. This estimation revealed that the axial flow through the propeller disk is approximately twice the magnitude of the axial flow near the boundary (the free-stream velocity). As noted in Table 1, the axial velocity at the inflow plane is 5.833 ft/s, so the approximate axial velocity through the propeller is 11.667 ft/s. Based on this

assumption, some calculations were performed to determine the size of a vortex necessary to affect the blades on the time scale shown by the side force results in Figure 28.

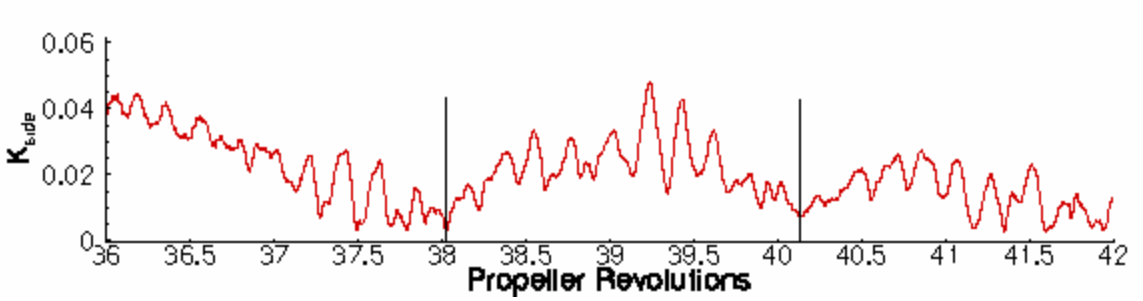


Figure 28- Portion of side force results from LES.

These results display a peak in side force over the course of approximately 2.1 revolutions. The P4381 used for this analysis has blades that have an axial length of approximately 3.0 inches. In order for a vortex to affect the blades long enough to result in the peak seen in Figure 28, the vortex must be over 2.0 feet long. No vortex cores were observed to be anywhere near this magnitude in any of the animations, so the pressure fluctuations must be a result of a steady increase and decrease in the number of created or ingested vortices over a short period of time rather than single, intense vortices passing through the propeller disk. This increase and decrease could be a function of the vortex ring's three dimensional motion, deformation, and shedding. It has been shown by Stettler (2004), Gharib *et al.* (1998), and Krueger and Gharib (2003) that vortex rings have a finite circulation limit above which they shed. Any asymmetries in the vortex ring would induce azimuthal inhomogeneities in the propeller inflow, which, in turn, would cause asymmetries in the blade pressures. The animations created for this research provide a look at the overall trend of vortex movement; however, it is not possible to track individual vortices or quantify their existence using these visualizations. This would be an excellent topic for future crashback research.

# 4 CONCLUSIONS

This research served two purposes. First, the research validated the accuracy of the Large Eddy Simulation model against experimental data. The LES model showed that the mean, standard deviation, and root mean square values for calculated quantities such as thrust, torque, and side force compared well with those from experimental measurements. The CFD model also showed that the frequency of the force and torque oscillations correlated well with experimental data. There were anomalies in the LES results, but these can be explained by the limitations of the computational model. For instance, the model does not account for the cavitation or mechanical vibrations present in physical experiments. There are also limited computational results available, so it is difficult to determine long-term, low-frequency trends in the flow. These are both excellent areas for future research. Now that this model has been shown to accurately model the crashback scenario, it can be made more complex and realistic. This could be accomplished by adding complexities to the scenario, such as a propeller duct or a portion of a submarine hull. The model could also be manipulated to represent the effects of cavitation. Also, more revolutions for this advance ratio could be computed in order to evaluate low-frequency trends. This research should also be performed on LES (and other CFD techniques) results for other combinations of axial velocity and propeller speed, resulting in both similar and different advance ratios, to determine the effect of both axial velocity and propeller speed on the results. Now that this particular LES model has been shown to be accurate, it could be adapted to model a wide range of physical models and flow conditions.

Many of the theories evaluated in this research did not necessarily find support from the flow visualizations created, but many of these theories could still have an indirect effect on the forces and moments that occur during crashback. For example, the ring vortex density and orientation were both found to have little, if any, effect on the side force. The pressure fluctuation animations indicated that changes in pressure correlated well with the side force direction, and the vortex core animations indicated that the pressure distribution on the blade surfaces is affected by the presence of vortices. The blade section animations did indicate the ingestion of vortices into the propeller plane, so it is possible that the ring vortex could be the

origin of the vortices that result in the side force. The location of leading edge vortices on the blades did not directly correlate with the side force magnitude or direction; however, the blade section and pressure core animations showed that these could be related to the vortical regions that cause the pressure variations on the blade surfaces that were found to correlate with the side force.

If the pressure variation on the blades is affected by the ingestion of vortices, as theorized, then the high frequency responses (those in the vicinity of the blade rate) are likely due to pressure fluctuations on multiple blades as they rotate through vortices. The lower frequency responses would likely be due to the magnitude of the ingested vortices and the speed at which they pass through the propeller plane. The presence of large vortices results in larger side forces due to the magnitude of the pressure variations on the propeller blades. The speed at which these vortices traverse this region determines how long the blades will be affected by the vortices, thus affecting the frequency of these resultant forces. This research was not designed to quantify these results, but the qualitative analysis of these flow structures strongly suggests that the pressure fluctuation on the blade surfaces correlates with the side force.

This research will prove to be a valuable and important step in the continuing evaluation of the crashback maneuver, particularly indicating areas for future work. There are many possibilities for the next stage of crashback research. First, the flow field downstream of the propeller could be analyzed to evaluate the existence and movement of vortices that are or could be ingested into the propeller plane. The origin of these vortices must also be discovered. Whether they are a result of the leading edge pressure differential, vortex ring shedding, or a product of another velocity gradient elsewhere in the flow, the origin of these vortices must be determined in order to eventually develop means of controlling or eliminating them. Based on qualitative observations of the blade geometry it is highly likely that the side forces are generated in the root area on the blades which extend perpendicular to the resultant side force. As mentioned previously, the pressure force on the blades was not able to be calculated in Ensight, because of a bug in Ensight. Future research should utilize the corrected Force function in order to quantitatively determine which portions of the blade surfaces have the greatest effect on the side force and then to correlate them with the velocity fields and ring vortex. This would be an

excellent way to determine the contribution, if any, of the mean pressure distribution to the side force and compare it to the contribution of the pressure fluctuations.

This research was never designed to solve the crashback problem completely, but it was organized such that it would provide sufficient information to support further research. This is a very early step in a long series of research projects meant to ultimately solve the crashback phenomenon through computational methods. The LES code evaluated was shown through a thorough validation process to provide accurate results as compared to similar physical experiments. With the CFD results validated, steps were taken to visualize many aspects of the flow field in hopes of discovering relationships between the flow structure and the quantifiable results. This research evaluated many ideas, some theories from experimentalists, some from other computationalists, and some from this particular project. Many of these ideas were found to have little support from flow visualization, and others were born out of these particular animations and illustrations. This research was successful in contributing to the foundation of crashback knowledge and supporting the future of crashback research.

# LIST OF FIGURES



# LIST OF TABLES

# REFERENCES

Bridges, B.H., Martin Donnelly, and Joel Park, "Experimental Investigation of the Submarine Crashback Maneuver," 43rd AIAA Aerospace Sciences Meeting and Exhibit, Reno, Nevada, 10-13 January, 2005.

Gharib, Morteza, Edmond Rambod, and Karim Sharif, "A Universal Time Scale for Vortex Ring Formation," J. of Fluid Mechanics, Vol. 360, 1998, pp. 121-140.

Krueger, Paul S. and M. Gharib, "The Significance of Vortex Ring Formation to the Impulse and Thrust of Starting Jet," Physics of Fluids, Vol. 15, No. 5, 2003, pp. 1271-1281.

Jessup, S.D., David Fry, and Martin Donnelly, "Unsteady Propeller Performance in Crashback Conditions With and Without a Duct," 26th Symposium on Naval Hydrodynamics, Rome, Italy, 17-22 September, 2006.

Stettler, J.W., "Steady and Unsteady Dynamics of an Azimuting Podded Propulsor Related to Vehicle Maneuvering," PhD Thesis, Massachusetts Institute of Technology, 2004.

Višohlíd, M. and Krishnan Mahesh, "Large Eddy Simulation of Crashback in Marine Propellers," 26th Symposium on Naval Hydrodynamics, Rome, 2006.

Višohlíd, M. and Krishnan Mahesh, "Large Eddy Simulation of Propeller Crashback," RTO-MP-AVT-123, Symposium on Flow Induced Unsteady Loads and the Impact on Military Applications, Budapest, 2005.